148
10-6-81

(2)
B7538

LA-3080

MASTER

ORNL/TM-7891

ornl

OAK
RIDGE
NATIONAL
LABORATORY

UNION
CARBIDE

Pressure Drop and Heat-Transfer Correlations for Use in CFTL Bundle Analysis

S. A. Hodge L. Meyer

OPERATED BY
UNION CARBIDE CORPORATION
FOR THE UNITED STATES
DEPARTMENT OF ENERGY

ORNL/TM-7891
Dist. Category UC-77

Contract No. W-7405-eng-26

Engineering Technology Division

Gas-Cooled Fast Reactor Program
FTP 01352, GCFR Core Flow Test Loop

PRESSURE DROP AND HEAT-TRANSFER CORRELATIONS FOR USE IN CFTL BUNDLE ANALYSIS

S. A. Hodge L. Meyer

Date Published: October 1981

NOTICE This document contains information of a preliminary nature. It is subject to revision or correction and therefore does not represent a final report.

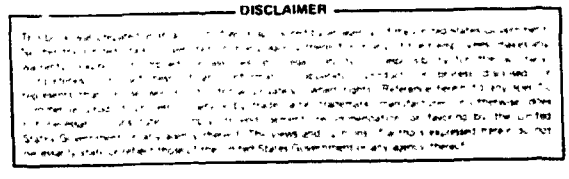

Prepared by the
OAK RIDGE NATIONAL LABORATORY
Oak Ridge, Tennessee 37830
operated by
UNION CARBIDE CORPORATION
for the
DEPARTMENT OF ENERGY

CONTENTS

	Page
ABSTRACT	1
INTRODUCTION	1
TURBULENT FLOW REGIMES	2
FRICTION FACTOR CORRELATION	2
TRANSITION REGION FLOW	5
EFFECT OF TEMPERATURE ON FRICTION FACTOR	10
HEAT TRANSFER CORRELATION	13
RESULTS FOR T_{WM} 150°C	15
RESULTS FOR T_{WM} 350°C	20
CONCLUSIONS	25
SUMMARY	26
NOMENCLATURE	27
REFERENCES	28
APPENDIX A	29
APPENDIX B	33
APPENDIX C	37

PRESSURE DROP AND HEAT TRANSFER CORRELATIONS FOR USE IN CFTL BUNDLE ANALYSIS

S. A. Hodge L. Meyer*

ABSTRACT

The friction factor and Stanton number for flow past a roughened surface are determined by the parameters A and $R(h^+)$ of the universal law of friction and the parameters A_H and $G(h^+)$ of the universal law of heat transfer. The methods used for experimental determination of these parameters for the particular roughness and rod diameter proposed for use in the Core Flow Test Loop (CFTL) are presented and recommended values for use in CFTL bundle flow analysis are prescribed.

INTRODUCTION

The Core Flow Test Loop (CFTL) was designed at Oak Ridge National Laboratory (ORNL) to be a high temperature, high pressure system for the circulation of helium coolant in axial flow through a bundle of electrically heated fuel rod simulators (FRS) under steady state and transient conditions. The fuel rod simulators were designed to be typical of GCFR application, with the cladding surface roughened over the heated length.

The initial test rod bundle planned for installation in the CFTL was a 37 rod bundle consisting of 34 roughened and heated FRS plus three larger-diameter, roughened but unheated grid spacer support rods. This bundle is enclosed in a smooth hexagonal duct; its construction is shown in Fig. 1 of Ref. 1 and comprises four types of flow channel. These are:

1. central channels, bounded by three heated FRS;
2. support rod channels, bounded by two heated FRS and an unheated spacer grid support rod;
3. wall channels, bounded by two FRS and the smooth duct wall; and
4. corner channels, bounded by one FRS and an interior angle of the duct wall.

The ratio of the velocity profile width to the roughness rib height is important to the determination of the friction factor and Stanton number for flow past a particular roughened surface. A profile of the actual roughness machined on the CFTL FRS cladding surface is shown in Appendix A; this roughness has a trapezoidal shape, a roughness rib height of 0.13 mm, a pitch-to-height ratio of 12, and a width-to-height ratio of 3.5. These dimensions produce a volumetric radius† of 3.918 mm for the CFTL fuel rod simulators and a volumetric radius of 4.718 mm for the larger-diameter unheated grid spacer support rods.

The velocity profile width is defined as the separation distance between the volumetric surface of a roughened rod and the surface of zero net momentum transfer, or shear, in the adjacent flow. This distance varies among the four CFTL channel types due to the differing geometries. In the wall and corner channels, it is also a function of the flow because the surface of zero shear moves outward from the roughened rod surface toward the smooth duct wall as the Reynolds number increases.[2]

*Technical staff member, Kernforschungszentrum Karlsruhe (KfK).

†The volumetric radius of a roughened rod is defined as the radius which would prevail if the volume of the roughness elements were smeared evenly over the rod surface.

In view of the wide range of velocity profile widths which would exist simultaneously within the various channels of the proposed CFTL test bundle, it was deemed essential to an accurate analysis of the CFTL flows that correlations expressing the dependence of friction factor and Stanton number upon velocity profile width be established experimentally for the particular CFTL roughness. The experiments to this purpose were conducted at KfK, Karlsruhe, FRG.

TURBULENT FLOW REGIMES

It was shown by Nikuradse[3] that turbulent flow* past a roughened surface can be characterized by one of three flow regimes, depending on the nature of the variation of the friction factor with the Reynolds number of the flow. At relatively low flow in the turbulent range, the friction factor varies with the Reynolds number in the same manner as in turbulent flow past a smooth surface, and the flow is said to be "hydraulically smooth." As the Reynolds number is increased, the thin region near the wall in which the flow field is dominated by the fluid viscosity narrows so that the roughness elements protrude to an increasing extent into the main flow stream, generating an increased frictional pressure loss by the mechanism of form drag. After this "transition region," the roughness elements are fully exposed to the main flow stream and the frictional pressure loss is virtually all due to form drag. Thus, at sufficiently high Reynolds numbers, the friction factor becomes independent of the Reynolds number and the flow characterized by a constant friction factor is termed "fully rough."

Each of these three turbulent flow regimes would exist within the roughened portion of the CFTL bundle at some time during the planned test schedule. For tests at low bundle flow, fully rough flow would exist in the central and support rod channels concurrent with transition region and/or hydraulically smooth flow in the wall and corner channels.† While existing relations applicable to flow past smooth walls could be used in the analysis of hydraulically smooth flow within the CFTL bundle, there was a need for development of correlations for the variation of friction factors and Stanton numbers with velocity profile width in both the transition and fully rough regimes of flow. It was also important to establish the Reynolds number range in which each correlation applies, that is, to establish the extent of the transition region.

FRICTION FACTOR CORRELATION

A friction factor for flow past roughened surfaces is defined in a manner similar to that for smooth surfaces. The friction factor for rough surface flow is defined as the proportionality factor f_i in the equation

$$\tau_w = f_i \frac{\rho_i \bar{u}_i^2}{2} . \tag{1}$$

for the axially averaged shear stress τ_w at the rough wall. The terms ρ_i and $\bar{u}_i$ in this equation represent the density and the spacially averaged velocity for the flow between the rough wall and the surface of zero shear in the adjacent flow.

---

*Laminar flow past a roughened surface can be treated in the same manner as laminar flow past a smooth surface, except that the flow passage should be considered to be that defined by the roughness rib tips.

†The wall and corner channels are bounded by both rough (rod) and smooth (duct wall) surfaces. By design, these channels have much larger wetted perimeters and consequently, significantly lower Reynolds numbers than the bundle average.

The friction factor f_1 can be related to the velocity profile width Y_L in the adjacent flow by the universal law of friction for flow past rough surfaces.[2] For flow in an annular geometry such as that formed by axial flow over the surface of one of the rough rods in a rod bundle, this law can be written as the linear equation

$$\sqrt{2/f_1} = A\left[\ln (Y_L/h) - \frac{1}{2} - \frac{1}{2 + Y_L/r_1}\right] + R(h^+) . \tag{2}$$

The term h in Eq. (2) represents the height of the roughness rib above the root, while r_1 is the volumetric radius of the rough rod. The parameters A and $R(h^+)$ are independent of Reynolds number in fully rough flow. Mathematically, the parameter A is the gradient of the linear portion of the dimensionless velocity profile while $R(h^+)$ is the value of the dimensionless velocity at a point h units above the surface. However, recent experiments by Meyer and Vogel[5] in a parallel plate geometry have shown that the gradient of the linear portion of the dimensionless velocity profile varies with the velocity profile width and can differ significantly from the slope A of the linear relation of Eq. (2). This discrepancy is probably due to the known physical deviation of the dimensionless velocity profile from linearity both near the rough wall and near the surface of zero shear. The effect of these deviations on the average value of the dimensionless velocity, which is directly related to the friction factor by the equation

$$\bar{u}_1^+ = \sqrt{2/f_1} , \tag{3}$$

will vary with the velocity profile width since a smaller fraction of the dimensionless velocity profile will be linear in a small channel with a short velocity profile.

In fully rough flow, the parameters A and $R(h^+)$ of Eq. (2) become constant values. These values have been determined for the CFTL roughness by testing a single prototype rod in three different annular geometries; each geometry was formed by placing the rough rod at the center of one of a series of three smooth tubes of varying diameter. A discussion of the experimental apparatus and procedure is provided in the appendix.

The friction factors f_1 and the corresponding velocity profile widths (Y_L) were determined for various flows adjacent to the rough rod in each of the three annular geometries using the experimentally measured values for axial pressure drop and flow, and application of the Dalle Donne-Meyer transformation.[6,7] The slope A and intercept $R(h^+)$ of Eq. (2) were then determined by plotting the friction factor term $\sqrt{2/f_1}$ as a function of the velocity profile width term given by

$$\left[\ln (Y_L/h) - \frac{1}{2} - \frac{1}{2 + Y_L/r_1}\right] . \tag{4}$$

The graphical interpretation for the results representative of fully rough flow is shown in Fig. 1.

Three distinct clusters of points are shown in Fig. 1. Each cluster contains the points representative of isothermal axial flow past the CFTL rod in one of the three smooth outer tubes, over a range of Reynolds numbers in the fully rough flow regime. The parameter Y_T (mm), which represents the distance from the volumetric surface of the rough rod to the inner surface of the smooth tube, is indicated for each of the three annular geometries. As delineated in Fig. 1, the intercept $R(h^+)$ and slope

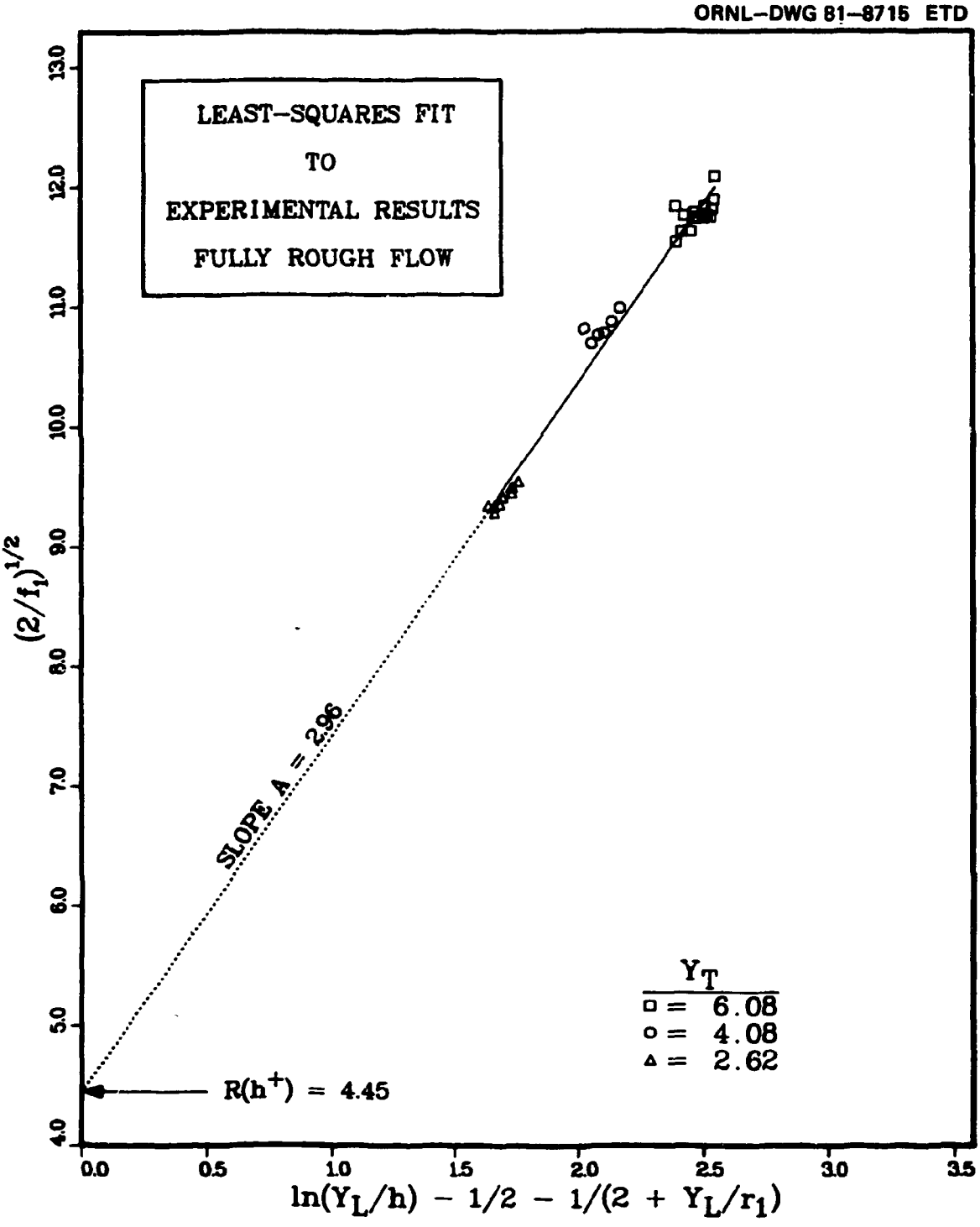

Fig. 1. The universal law of friction for the CFTL rod.

A for use in Eq. (2) for calculation of the friction factors within the CFTL bundle in fully rough flow have values of 4.45 and 2.96, respectively.

TRANSITION REGION FLOW

The parameters $R(h^+)$ and A become constant in fully rough flow because the friction factor is independent of the Reynolds number; this is not the case for flows within the range of the transition region. The friction factor can be expressed as a function of the Reynolds number, but it is more common to characterize flow in the transition region as a function of the roughness Reynolds number h^+, where

$$h^+ = \frac{hu^*}{\nu} = \frac{h}{D} \, Re \, \sqrt{f_i/2} \, . \tag{5}$$

The roughness Reynolds number is preferred because it is not a function of the hydraulic diameter. Thus, for single-rod tests in a succession of annular geometries with differing hydraulic diameters, the flow will become fully rough at different Reynolds numbers, but at the same value of h^+, since the roughness height would not change in these tests.

The procedure employed to determine values for the parameters $R(h^+)$ and A for use in Eq. (2) for flows in the transition region is basically the same as that used for fully rough flow. However, to prepare a graph of Eq. (2) in the transition region, it is necessary that each ordinate value $\sqrt{2/f_i}$ be plotted as a function of the abcissa value [Eq. (4)] which corresponds to the same roughness Reynolds number (h^+). To this end, it is useful to first separately plot the ordinate and the abcissa values as functions of h^+.

A semilogarithmic plot of the ordinate values $\sqrt{2/f_i}$ as a function of h^+ for the CFTL rod is shown in Fig. 2. Each of the three curves represents the experimental results for a different annular geometry; the parameter Y_i (mm) that differentiates the curves is the annular gap, which is the distance between the volumetric surface of the rough rod and the inner surface of the smooth outer tube. The nearly vertical lines which indicate a rapid decrease in the friction factor (f_i) with increasing h^+ at very low values of h^+ are least-squares fits to the experimental results obtained for laminar flow. Following the transition to turbulent flow, it can be seen that the friction factor (f_i) increases with h^+ in the transition zone, then becomes constant (within the limits of experimental error) as the flow becomes fully rough at an h^+ value of about 20.

The curved lines representing the results for flow in the transition region are least-squares fits to the plotted data for the two smaller annular geometries. However, for the uppermost curve which represents the results for flow in the 20 mm ($Y_i = 6.08$ mm) geometry, the least-squares fit was derived without consideration of the three points lying in the range of h^+ values between 3 and 9; these points can be seen to lie significantly below the uppermost dotted line. Subsequent to completion of the isothermal tests in the 20 mm smooth tube, the pressure transducer used for some of the readings at low flows was found to be out-of-calibration; this is believed to be the source for the anomalous behavior of the experimental results for low isothermal flow in the 20 mm tube. Fortunately, the geometries of the four channel types included in the CFTL bundle design would result in velocity profile widths which lie between those in the two smaller annular test geometries.

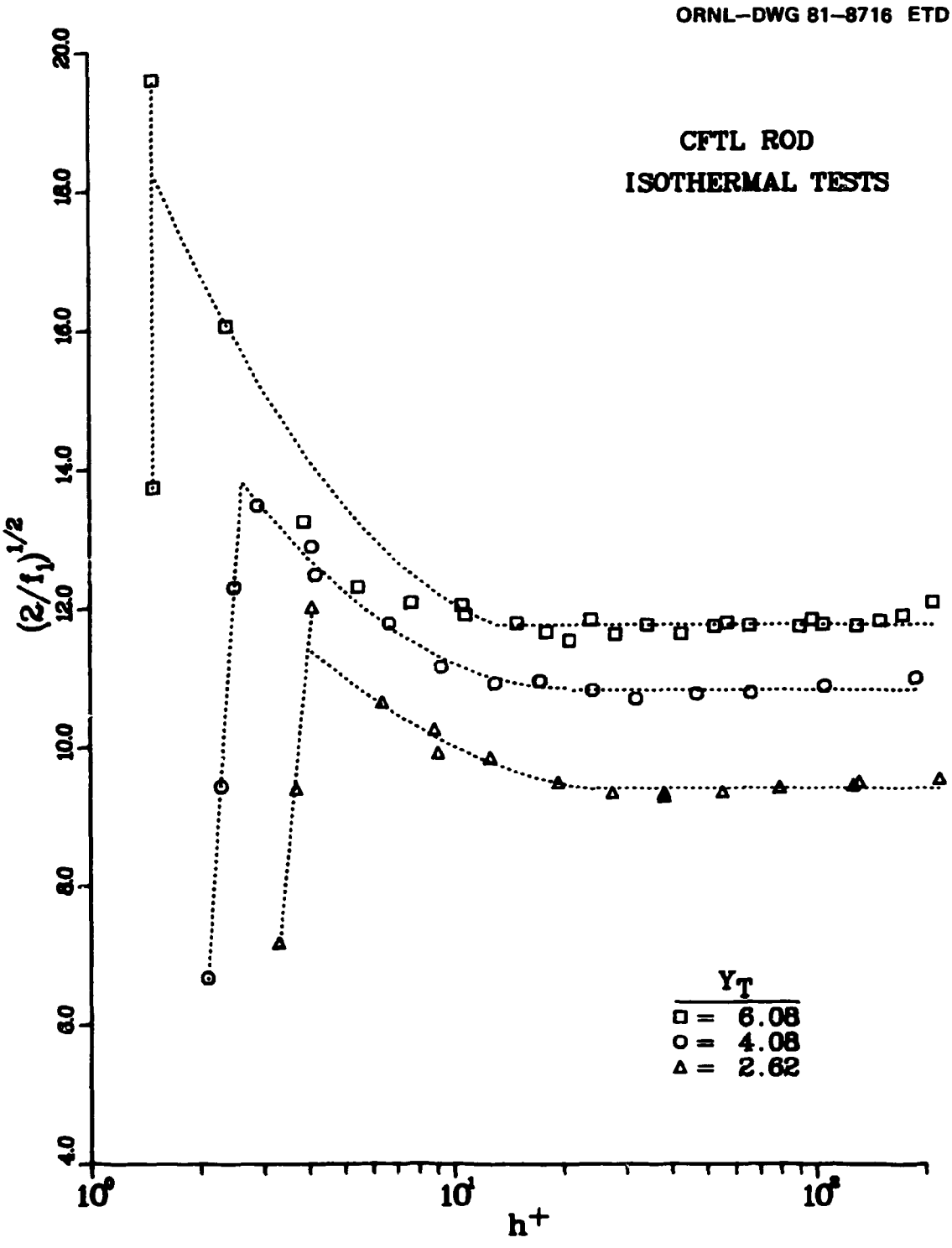

Fig. 2. Variation of ordinate values with roughness Reynolds number in the transition zone.

The correlation for the least-squares curve-fits to the transition zone results shown in Fig. 2 are of the form

$$\sqrt{2/f_t} = C_1 + C_2 \ln (h^+) + C_3[\ln (h^+)]^2 , \tag{6}$$

The values of the constants for use in Eq. (6) for each of the annular test geometries are listed in Table 1. It is also important to note from the results displayed in Fig. 2 that the transition zone for flow within the channels of the CFTL bundle can be expected to extend over the range of roughness Reynolds numbers (h^+) from about 3 to 20.

Table 1. Constants for the correlation of $\sqrt{2/f_t}$ with $\ell n(h^+)$ per Eq. (6)

Annular gap Y_T (mm)	C_1	C_2	C_3
6.08	20.527	−5.973	1.001
4.08	17.312	−4.283	0.710
2.62	17.868	−5.425	0.869

The values on the abcissa [Eq. (4)] are plotted as functions of h^+ on the semilogarithmic plot of Fig. 3. The modest but continuous increase in these values with h^+ is caused by a slight movement of the surface of zero shear outward from the rough rod toward the inner surface of the smooth tube as the velocity of the flow increases. It should be noted that this increase in the velocity profile width (Y_L) with the roughness Reynolds number occurs in fully rough flow as well, albeit at a reduced rate.

The constants for the correlation of Eq. (4), that is,

$$\ln (Y_L/h) - \tfrac{1}{2} - 1/(2 + Y_L/r_1) = C_4 + C_5 \ln (h^+) + C_6[\ln (h^+)]^2 \tag{7}$$

obtained by a least-squares fit to the curves of Fig. 3 are listed in Table 2.

Table 2. Constants for the correlation of Eq. (4) with $\ell n(h^+)$ per Eq. (7)

Annular gap Y_T (mm)	C_4	C_5	C_6
6.08	1.658	0.346	−0.035
4.08	1.323	0.324	−0.032
2.62	0.929	0.314	−0.030

Derived ordinate values can be plotted against the corresponding values on the abcissa at selected values of the roughness Reynolds number by using these least squares polynomial fits for both the ordinate and the abcissa terms of Eq. (2). The result is shown in Fig. 4 for four values of h^+ in the transition zone at uniform intervals ranging from 5 to 20. The lowest plotted line in this figure is

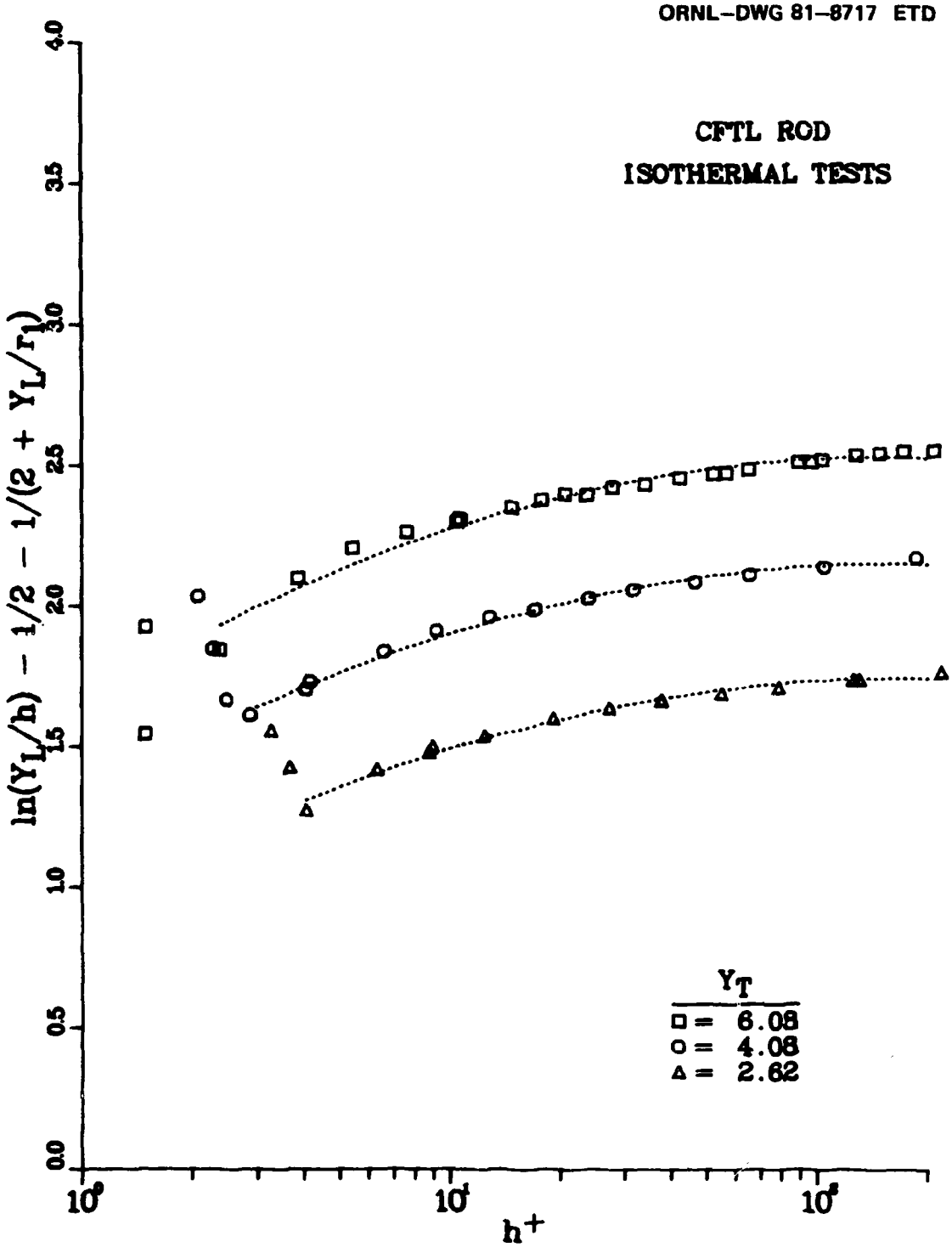

Fig. 3. Variation of abscissa values with roughness Reynolds number in the transition zone.

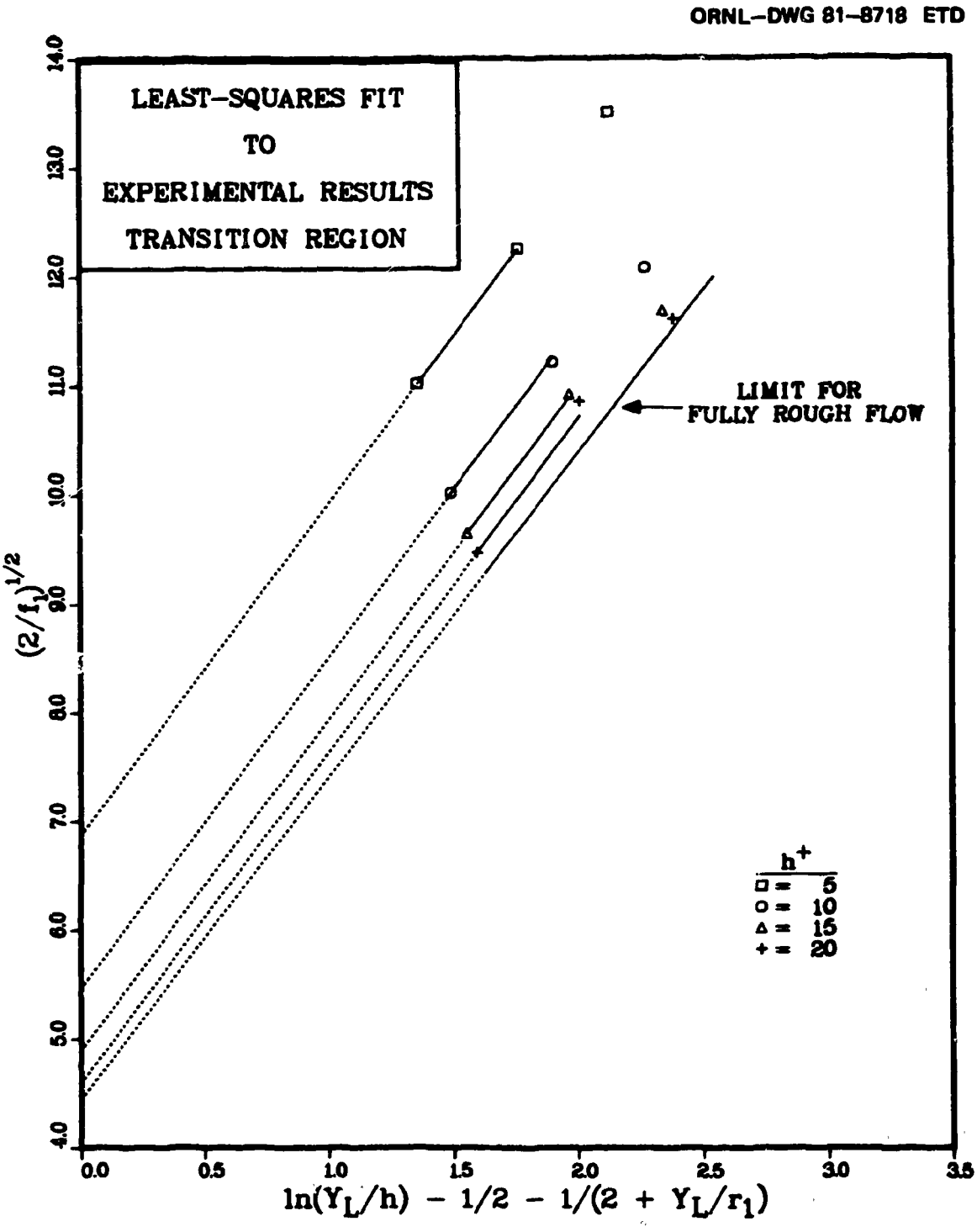

Fig. 4. The universal law of friction for the CFTL rod in the transition region.

identical to the line plotted in Fig. 1 and represents the limiting relation between $\sqrt{2/f_1}$ and Eq. (4) reached as the value of h^+ increases into the regime of fully rough flow.

In the transition region at h^+ values of 20 or below, the points plotted in Fig. 4 representing flow in the two smaller annular geometries have been connected by straight solid lines; these lines have been extended to the ordinate axis by dotted lines. As was illustrated in Fig. 1 for the case of fully rough flow, the slopes of these lines represent the parameter A and the ordinate intercepts represent the parameter $R(h^+)$ at the particular value of h^+ for which each line was drawn. The points representing transitional zone flow past the rough rod in the 20 mm smooth tube shroud were not considered in the establishment of these values because of the experimental difficulty mentioned previously and because the CFTL channel geometries lie between those of the two smaller annular test geometries.

As shown in Fig. 4, the roughness parameters for CFTL rod in the transition zone can best be modeled by the assumption that the slope A remains constant at the value obtained for fully rough flow,

$$A = 2.96 \tag{8}$$

with a corresponding dependence of the ordinate intercept upon the roughness Reynolds number given by

$$R(h^+) = 8.695 - 0.423\,(h^+) + 0.011\,(h^+)^2 \tag{9}$$

over the range $5 \leqslant h^+ \leqslant 20$. The use of these parameters in Eq. (2) will permit accurate determination of the friction factors for transition zone flow in any of the channels in the CFTL bundle design.

EFFECT OF TEMPERATURE ON FRICTION FACTOR

The previous discussion has concerned only the test results for isothermal flow. The term $\sqrt{2/f_1}$ is plotted as a function of h^+ for three different heating conditions within each of the smooth tube shrouds in Fig. 5. It should be noted that the scale of the ordinate is expanded, and there is no discernible effect of temperature for determinations with the 13-mm smooth tube shroud, denoted "shroud 13" on the figure. However, there is a slight decrease of friction factor with increasing temperature for flow in shroud 16, and a marked temperature effect is observed for the test results in shroud 20. Since the velocity profile widths for the various channels of the CFTL bundle fall between those modeled by shrouds 16 and 13, the expressions previously developed for determination of the parameters A and $R(h^+)$ in isothermal flow should give satisfactory results for a CFTL bundle flow analysis.

In Fig. 6, a temperature correction of the form

$$\sqrt{2/f_t} = \sqrt{2/f_t}\,(T_W/T_B)^{-0.10} \tag{10}$$

has been applied to all of the plotted data. This temperature correction is equivalent to the correction

$$f_t = f_t\,(T_W/T_B)^{-0.20} \tag{11}$$

and does reduce the scatter of data for the flows in shroud 20. However, as would be expected, this temperature correction spreads the originally closely grouped data for flow in the two smaller annular geometries and is therefore not recommended for CFTL application.

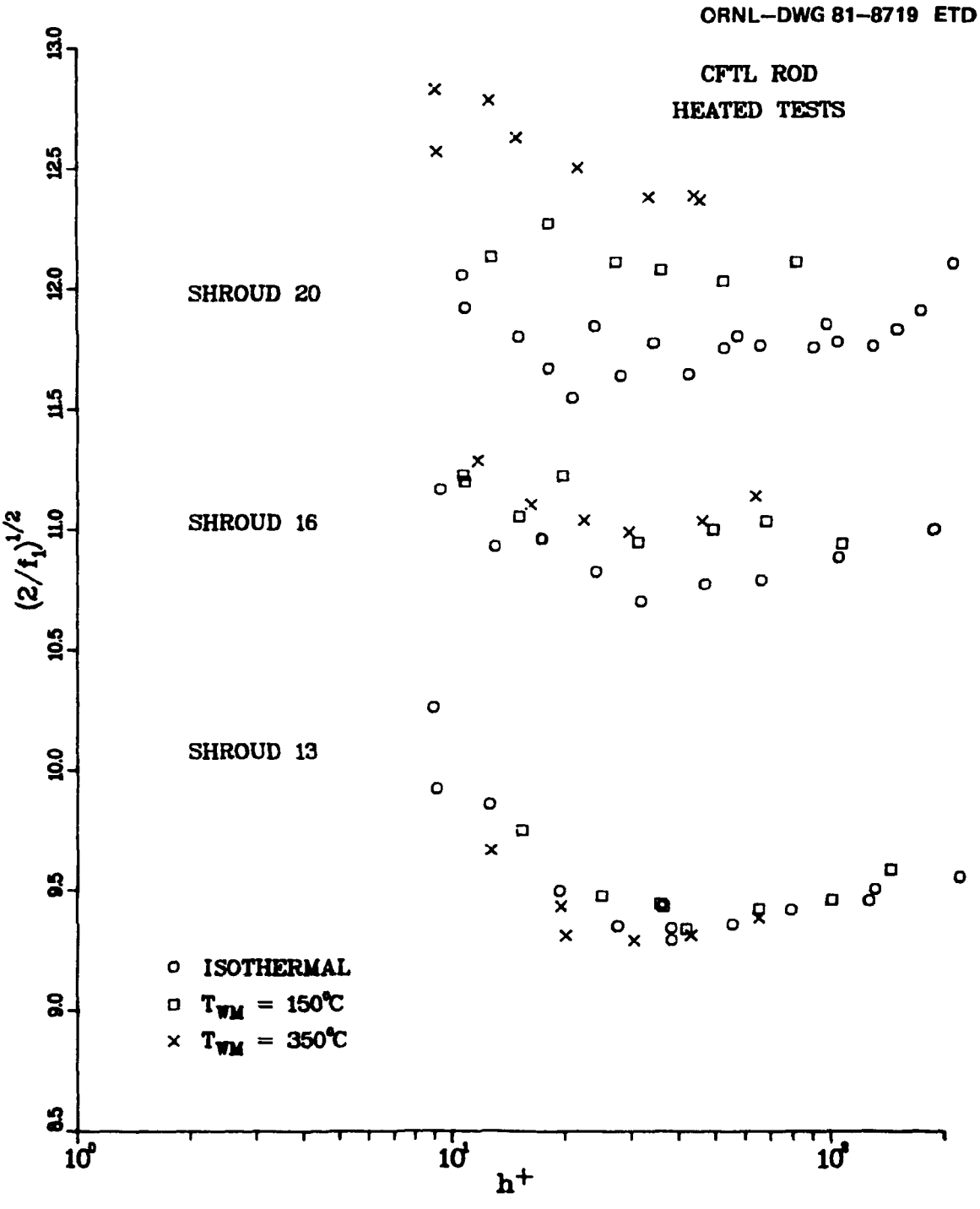

Fig. 5. Effect of temperature on ordinate values.

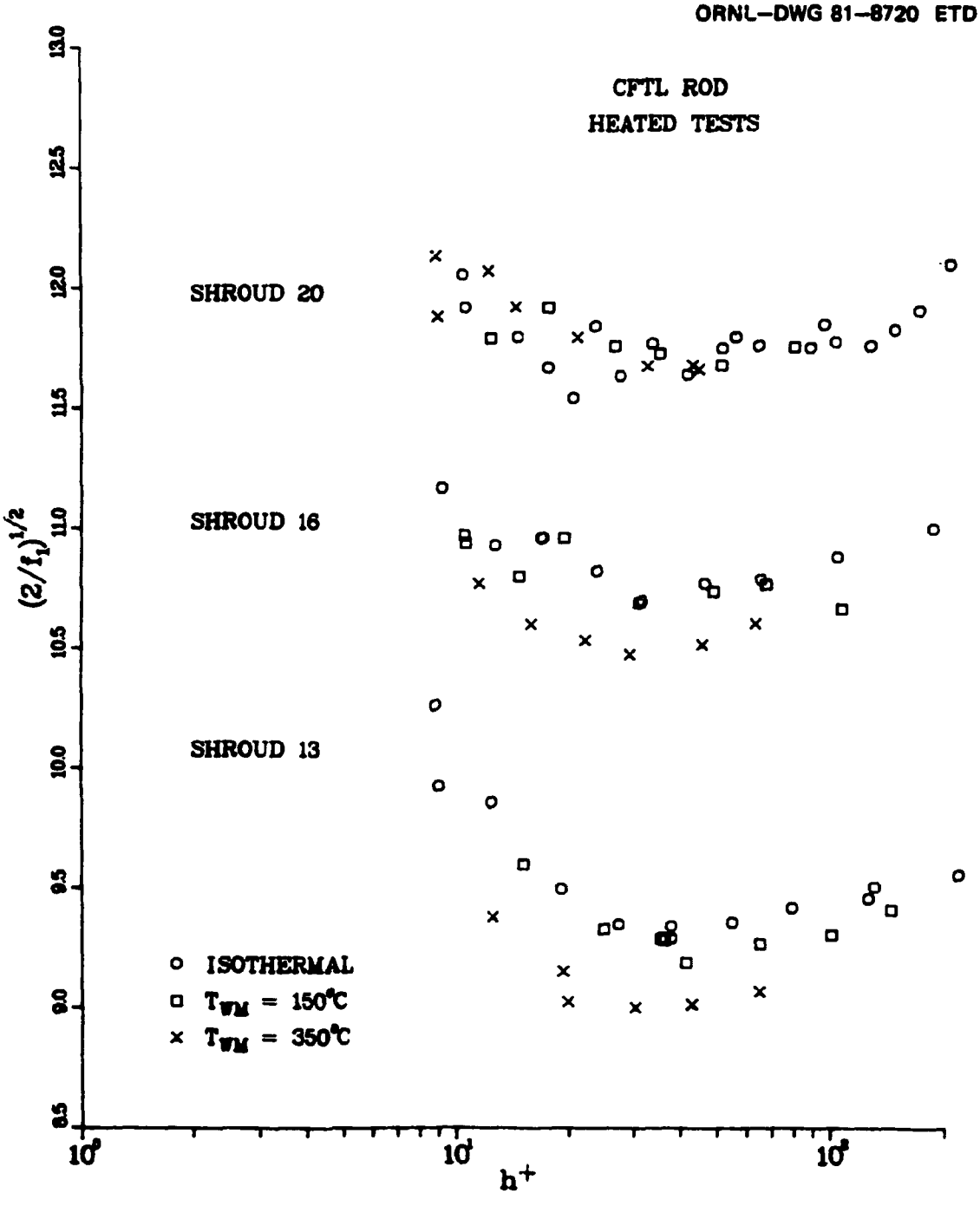

Fig. 6. Application of temperature correction to ordinate values.

HEAT TRANSFER CORRELATIONS

The universal law of heat transfer for flow in an annular geometry can be written in the form[2]

$$\frac{\sqrt{f_1/2}}{St_1} = A_H\left[\ln(Y_L/h) - \frac{1}{2} - \frac{1}{2 + Y_L/r_1}\right] + G(h^*) . \tag{12}$$

This law expresses the ratio of the term $\sqrt{f_1/2}$ to the Stanton number St_1, which is applicable to the region of flow between the volumetric surface of the rough rod and the surface of zero shear. This Stanton number is defined by the equation

$$St_1 = \frac{q_w}{(T_w - T_{B1})\,\rho_1\, C_p\, \bar{u}_1} , \tag{13}$$

where T_{B1} is the bulk temperature of the coolant in the region adjacent to the rough surface. It should be noted that the bracketed term on the right side of Eq. (12) is the same as that appearing in the universal law of friction for an annular geometry, Eq. (2).

The left side of Eq. (12) can be written in the form

$$\left(\frac{T_w - T_{B1}}{T_w - T_B}\right)\frac{(T_w - T_B)\,\rho C_p \bar{u}}{q_w}\,\frac{u^*}{\bar{u}}\,\frac{u_1^*}{u^*} \tag{14}$$

which is equivalent to the expression

$$\left(\frac{T_w - T_{B1}}{T_w - T_B}\right)\,\frac{\sqrt{f/2}\,u_1^*}{St\,u^*} . \tag{15}$$

where f and St are the friction factor and Stanton number for the overall annulus. The quantities f and St were directly determined from the experimental data, that is, no transformation was involved. The form of Eq. (15) is convenient because the ratio of friction velocities is easily evaluated using the relation[2]

$$\frac{u_1^*}{u^*} = \left(\frac{\beta - \alpha^2}{\alpha(1-\alpha)}\right)^{1/2} \cdot \left(\frac{\rho}{\rho_1}\right)^{1/2} . \tag{16}$$

The parameter α in Eq. (16) is the radius ratio* for the annular geometry, while β represents the ratio of the radius of the surface of zero shear to the radius of the smooth outer tube in which the rough rod is centered, and was calculated by the Dalle Donne-Meyer transformation.[6] The density ratio term of Eq. (16) was assumed sufficiently close to unity to be neglected.

*This is the ratio of the volumetric radius of the rough rod to the radius of the inner wall of the smooth tube and is equal to 0.392, 0.490, and 0.599 for the three annular geometries used in this experiment.

The value of the term on the left side of Eq. (12) was calculated for each heated set of experimental values in this analysis by performing the multiplication of the three terms as indicated in Eq. (15). The experimental results for each set of values are given in appendix C.

The parameters A_{II} and $G(h^*)$ of Eq. (12) are properties of the rough surface* and were determined for the CFTL rod in this experiment. Since the friction factor f_I is constant in fully rough flow and the Stanton number St_I monotonically decreases as h^* increases in this region[2], Eq. (12) shows that $G(h^*)$ must monotonically increase with h^* in fully rough flow. Conversely, in the transition zone both f_I and St_I increase with h^* so $G(h^*)$ will be relatively constant. These considerations show that the dependence of $G(h^*)$ upon the roughness Reynolds number is markedly different from the parameter $R(h^*)$ of the friction law, Eq. (2).

The graphical method used for determination of the slope A_{II} and intercept $G(h^*)$ of Eq. (12) is by construction of straight lines connecting the points representing the flows in the differing annular geometries used in the experiment. Since the wall intercept $G(h^*)$ is a function of the roughness Reynolds number, care was taken to ensure that each set of connected points represents results obtained at the same value of h^*.

The method used for determination of A_{II} and $G(h^*)$ is similar to that employed for determination of the analogous quantities for the friction law in the transition region. However, there is an important additional restriction on the utilization of the graphical procedure; this is due to the dependence of the coolant physical properties upon temperature. Since the experimentally determined friction factors and Stanton numbers are affected by the variation of coolant temperature across the annular gap, the experimental results used for the purpose of comparison in the different annular geometries should be obtained at approximately the same coolant bulk temperatures and wall-to-bulk temperature ratios (T_W/T_B). Two sets of comparable results were found for the CFTL rod heated flow experiments; each is characterized by the (controlled) maximum rod wall temperature. The maximum wall temperature (T_{WM}) and the range of wall-to-bulk temperature ratios for both sets of comparable results are listed in Table 3.

Table 3. Sets of comparable results obtained in the CFTL rod experiment

T_{WM}	Annular gap Y_T (mm)	T_W/T_B
150° C	6.08	1.31–1.34
	4.08	1.25–1.29
	2.62	1.17–1.21
350° C	6.08	1.71–1.79
	4.08	1.56–1.63
	2.62	1.35–1.43

To find the slope A_{II} and the intercept $G(h^*)$ of Eq. (12) graphically, values of the ordinate [on the left side of Eq. (12)] were plotted as a function of the corresponding values of the bracketed abcissa term on the right side. The corresponding plotted values represent flows within the different annular

*The parameter $G(h^*)$ is also a function of the Prandtl number and would therefore differ for the same roughness in different fluids.[1]

geometries at the same roughness Reynolds number so that the associated values of the wall intercept $G(h^+)$ are the same.

RESULTS FOR $T_{WM} = 150°C$

The set of curves for analysis of the heat flow results for a maximum rod wall temperature of 150° C are shown in Figs. 7–9. The ordinate terms obtained for the tests in the three different annular geometries are plotted as functions of the roughness Reynolds number in Fig. 7. The two straight-line approximations on this figure are least-squares fits to the plotted points representing flow in the 20-mm and 13-mm annular geometries, over the ranges indicated; a fit to the limited number of values available for flow in the 16-mm geometry was not attempted.

Values of the ordinate [on the left side of Eq. (12)] were obtained at the same value of h^+ for flow in the two different annular geometries by using the linear least-squares fitted equations indicated on Fig. 7. The abcissa values are shown in Fig. 8. The ordinate values from Fig. 7 and the abcissa values from Fig. 8 are plotted in the form of Eq. (12) at several values of h^+ in Fig. 9.

The slopes and ordinate intercepts of the straight lines shown on Fig. 9 are the values of A_H and $G(h^+)$ for Eq. (12) for the CFTL rod at the indicated roughness Reynolds numbers for the tests at a maximum wall temperature of 150° C. These quantities are listed as functions of h^+ in Table 4.

Table 4. Slopes A_H and ordinate intercepts for the straight lines of Fig. 9

h^+	A_H	$G(h^+)$
20	0.762	14.665
30	0.831	15.117
40	0.878	15.456
50	0.914	15.726
60	0.945	15.952
70	0.971	16.146
80	0.992	16.319
90	1.012	16.472
100	1.028	16.616

The slope A_H can be expressed as a function of the roughness Reynolds number h^+ by the relation

$$A_H = 0.645 + 6.9 \times 10^{-3}\, h^+ - 3.1 \times 10^{-5}\, (h^+)^2 . \qquad (17)$$

The values of $G(h^+)$ calculated from the experimental results in the CFTL rod heated tests with a maximum wall temperature of 150° C are shown plotted as a function of h^+ in Fig. 10. These points were calculated using Eq. (12) with experimentally determined values for the term $\sqrt{f_t/2}/St_t$ and the abcissa term of Eq. (4), and values of A_H as determined by Eq. (17). The plotted values are limited to those derived from the results of the heated tests for which the heat balance error* was no more than five percent.

*The heat balance error for each of the heated test runs is included in the calculated results tabulated in Appendix C.

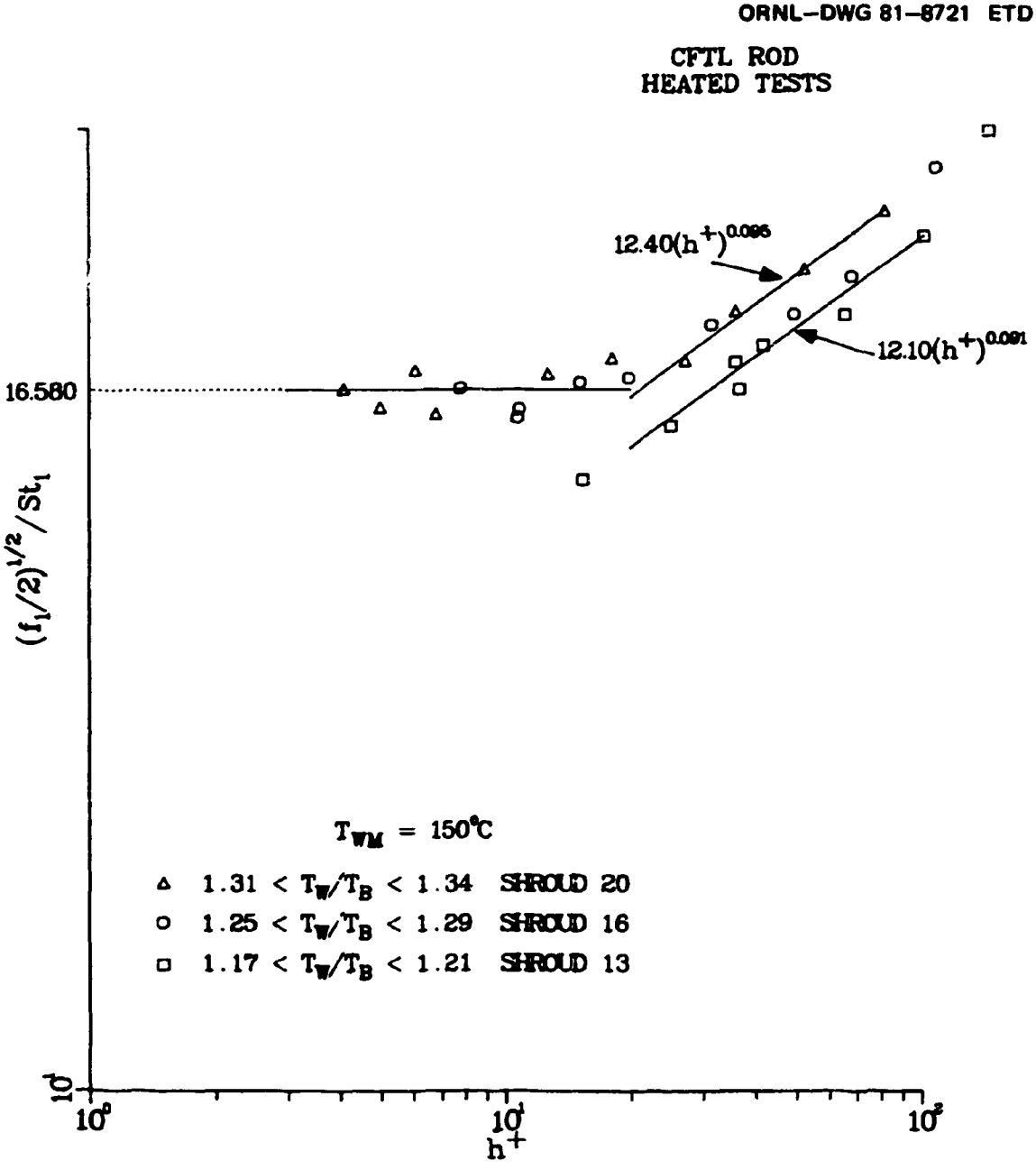

Fig. 7. Variation of ordinate values with roughness Reynolds number for flow with heat transfer.

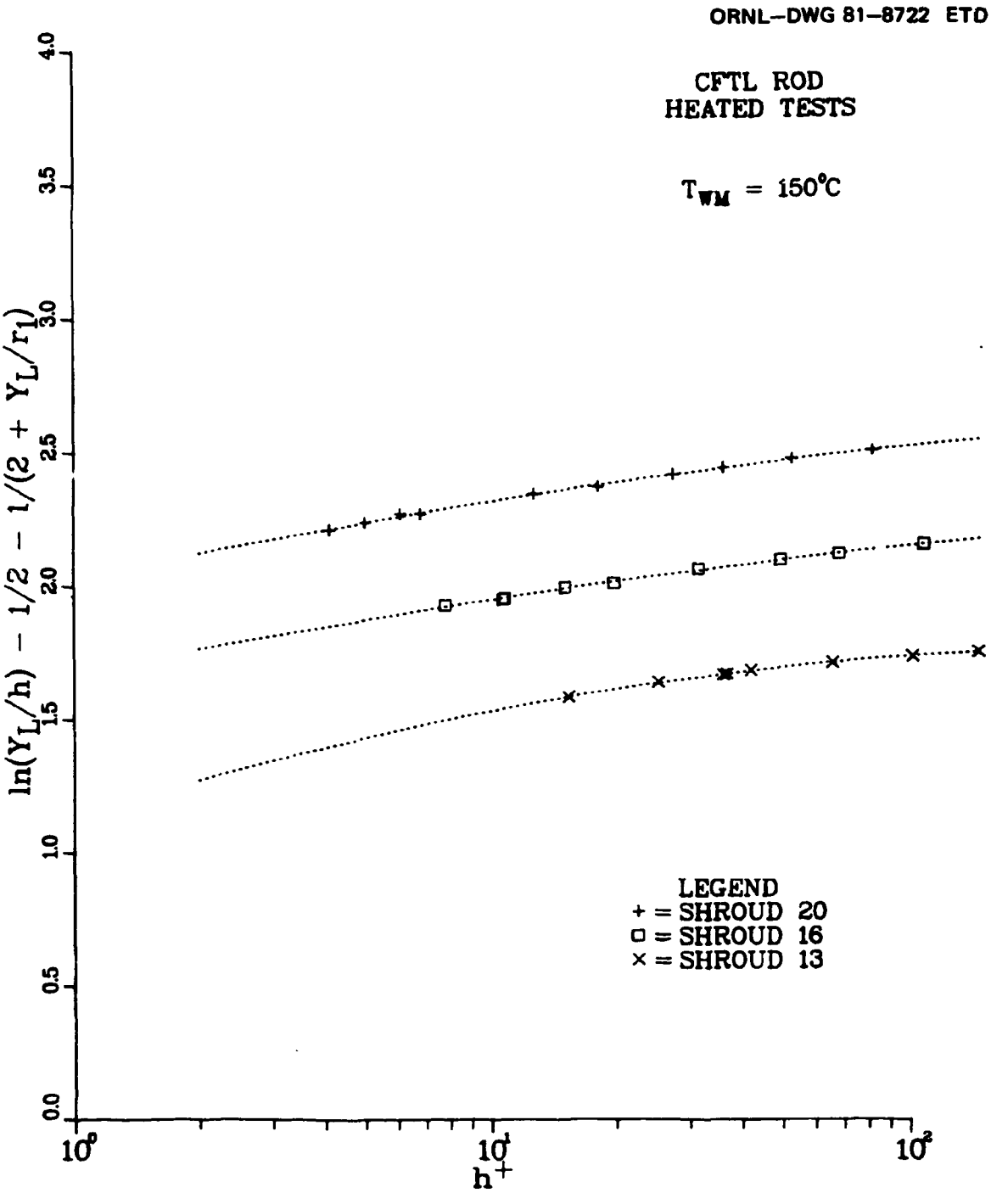

Fig. 8. Variation of abscissa values with roughness Reynolds number in the transition zone.

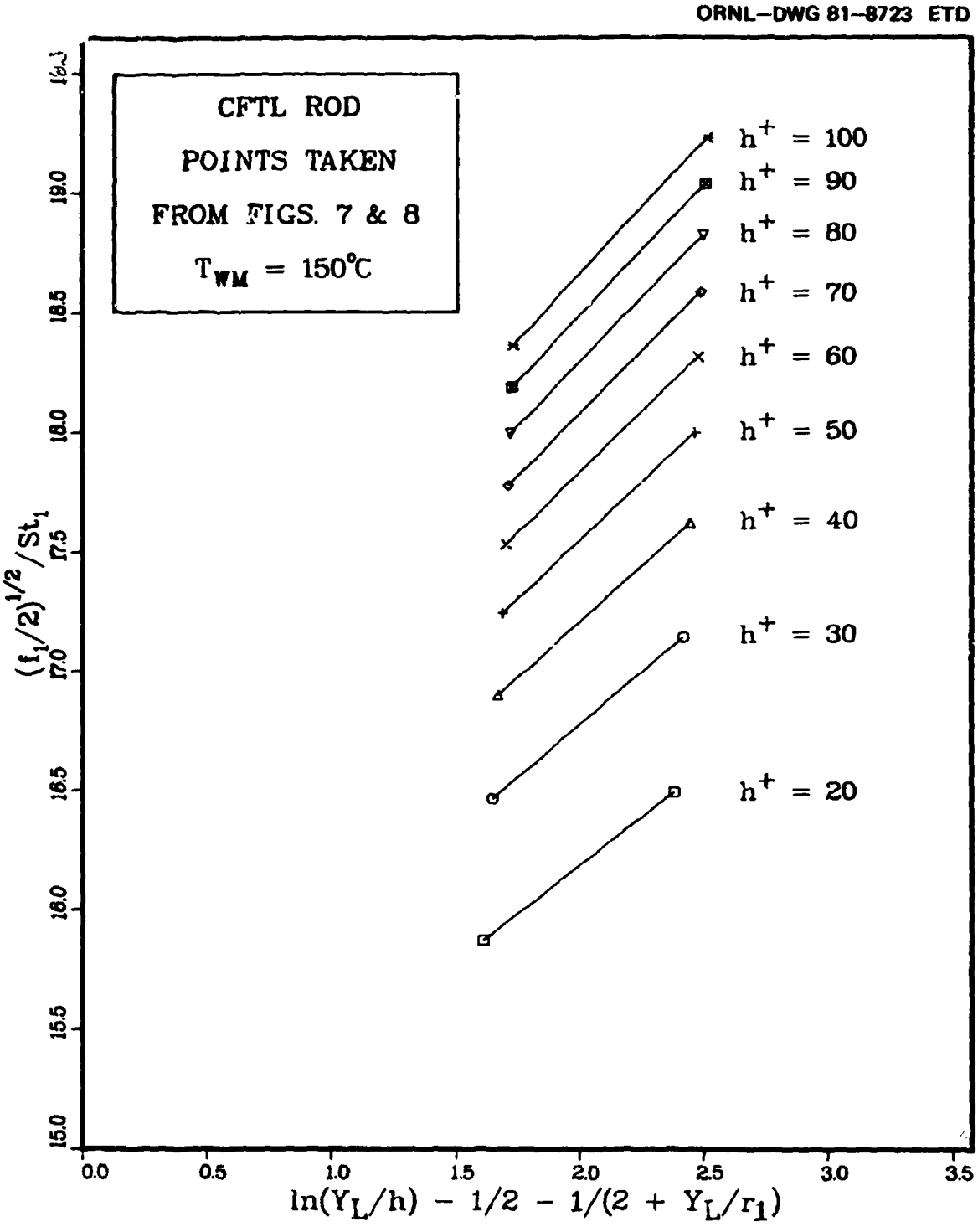

Fig. 9. Universal law of heat transfer for CFTL rod.

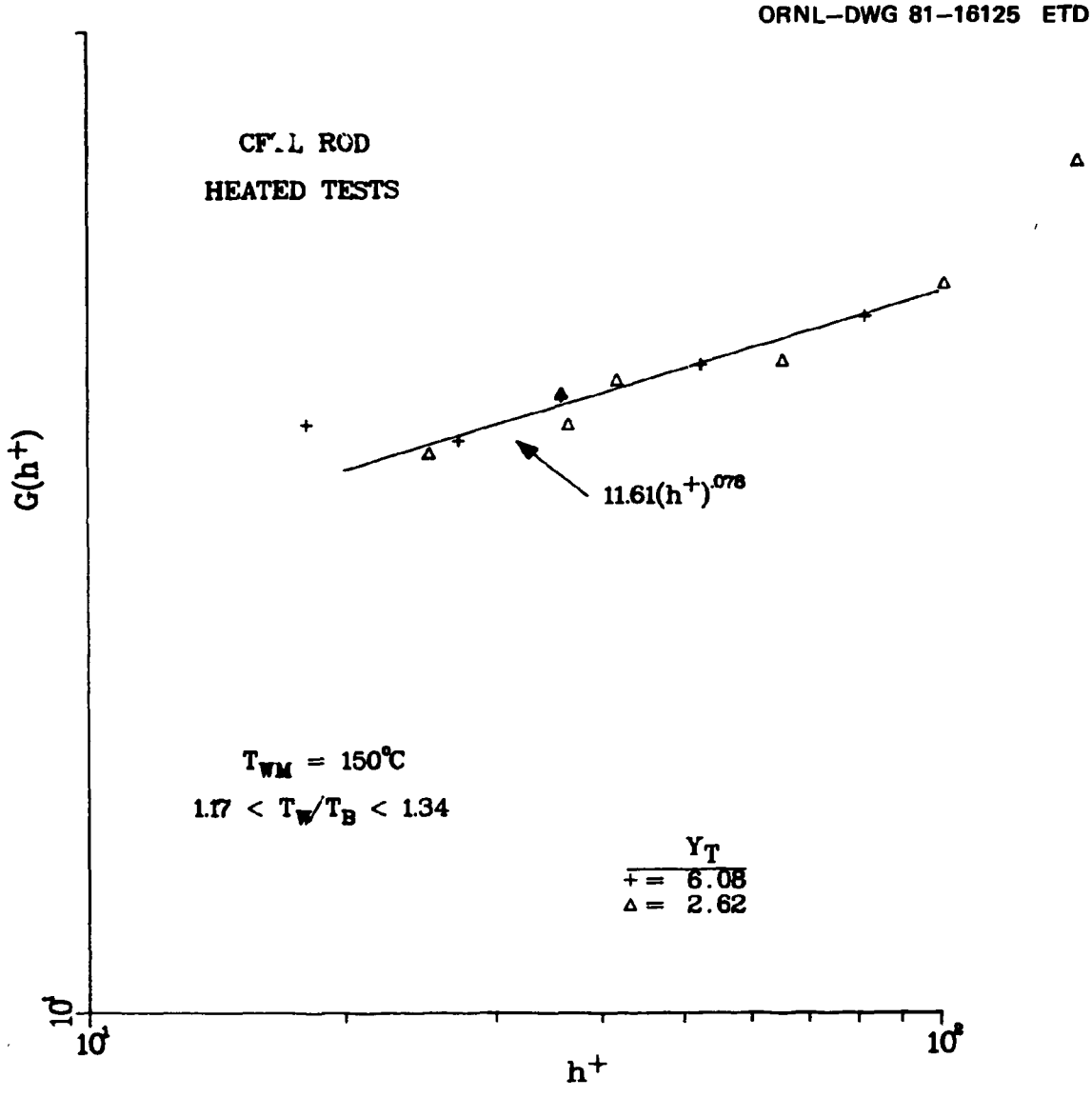

Fig. 10. Correlation for G(h*) using slopes determined graphically for the CFTL rod.

For values of h^+ less than 20, the flow is in the transition zone, and the value of the ordinate term is approximately constant and independent of the annular geometry as shown in Fig. 7. Accordingly, these experimental results show that once the friction factor has been determined, the Stanton number for use in CFTL analyses of transitional zone flow at T_{WM} of about 150° C can be calculated using the relation

$$(f_t/2)^{1/2}/St_t = 16.580 . \tag{18}$$

This relation should give satisfactory results over the range of roughness Reynolds numbers from the onset of turbulent flow, about $h^+ = 3$, to the beginning of the fully rough regime at about $h^+ = 20$.

RESULTS FOR T_{WM} = 350° C

The curves for the analysis of the experimental results for test runs with heated flow at a maximum rod wall temperature of 350° C are shown in Figs. 11-13. The ordinate terms obtained for the tests in the three different annular geometries are plotted as functions of the roughness Reynolds number in Fig. 11. The three straight-line approximations on the right side of this figure are least-squares fits to the plotted points representing flow at values of h^+ greater than about 9.0 in each of the annular geometries used in the experiment.

Values for the ordinate [on the left side of Eq. (12)] were obtained at the same value of h^+ for flow in the three different annular geometries by using the linear least-squares fit equations indicated on the right side of Fig. 11. The abcissa values are shown in Fig. 12.* The ordinate values from Fig. 11 and the abcissa values from Fig. 12 are plotted in form of Eq. (12) at several values of h^+ in Fig. 13.

As can be seen on Figs. 11 and 13, the plotted results for the flow in shroud 13 do not conform to the expected trend indicated by the results for the 16 and 20-mm shrouds. This may be due to the much larger spread of wall-to-bulk temperature ratios for the tests at a maximum rod wall temperature of 350° C†, or it may be due to an effect of undetected rod bowing at these higher temperatures in this smallest shroud. These anomalous results for the heated flow in shroud 13 at a maximum rod wall temperature of 350° C were not considered further in the analysis.

With the results for the flow in shroud 13 neglected, the slopes and ordinate intercepts of the straight lines connecting the points for flow in shrouds 16 and 20 are assumed to be the values of A_H and $G(h^+)$ for use in Eq. (12) for the tests at a maximum wall temperature of 350° C. These quantities are listed as functions of h^+ in Table 5.

The relation between the slope A and the roughness Reynolds number h^+ for the heated tests at a maximum wall temperature of 350 C as listed in Table 5 is well approximated by

$$A_H = 1.489 - 2.462 \times 10^{-2}\, h^+ + 1.109 \times 10^{-4}\, (h^+)^2 . \tag{19}$$

The values of $G(h^+)$ calculated from the experimental results in the CFTL rod heated tests with a maximum wall temperature of 350° C are shown plotted as a function of h^+ in Fig. 14. These points were calculated using Eq. (12) with experimentally determined values for the term $\sqrt{f_t/2}/St_t$ and the abcissa term of Eq. (4), and values of A_H as determined by Eq. (19). As before, the plotted values are limited to

---

*It is interesting to note that a comparison of Figs. 3, 8, and 12 indicates that there is no effect of temperature upon the abcissa values.

†Compare the spread of wall-to-bulk temperature ratios at a maximum rod wall temperature of 150° C, as given on Fig. 7. It would be necessary to heat the inlet flow to the test section foir tests in the larger annular geometries in order to reduce this spread.

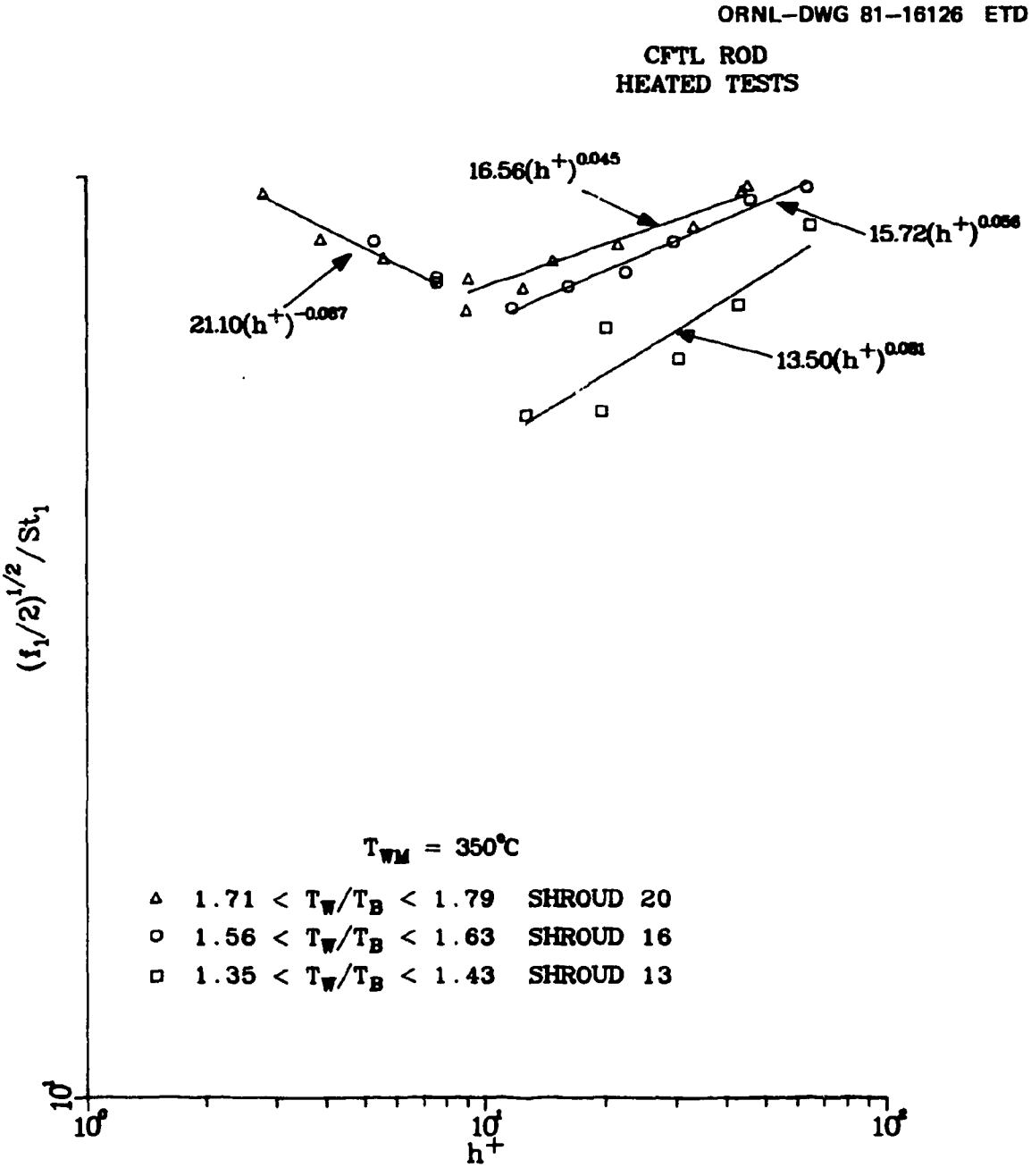

Fig. 11. Variation of ordinate values with roughness Reynolds number for flow with heat transfer.

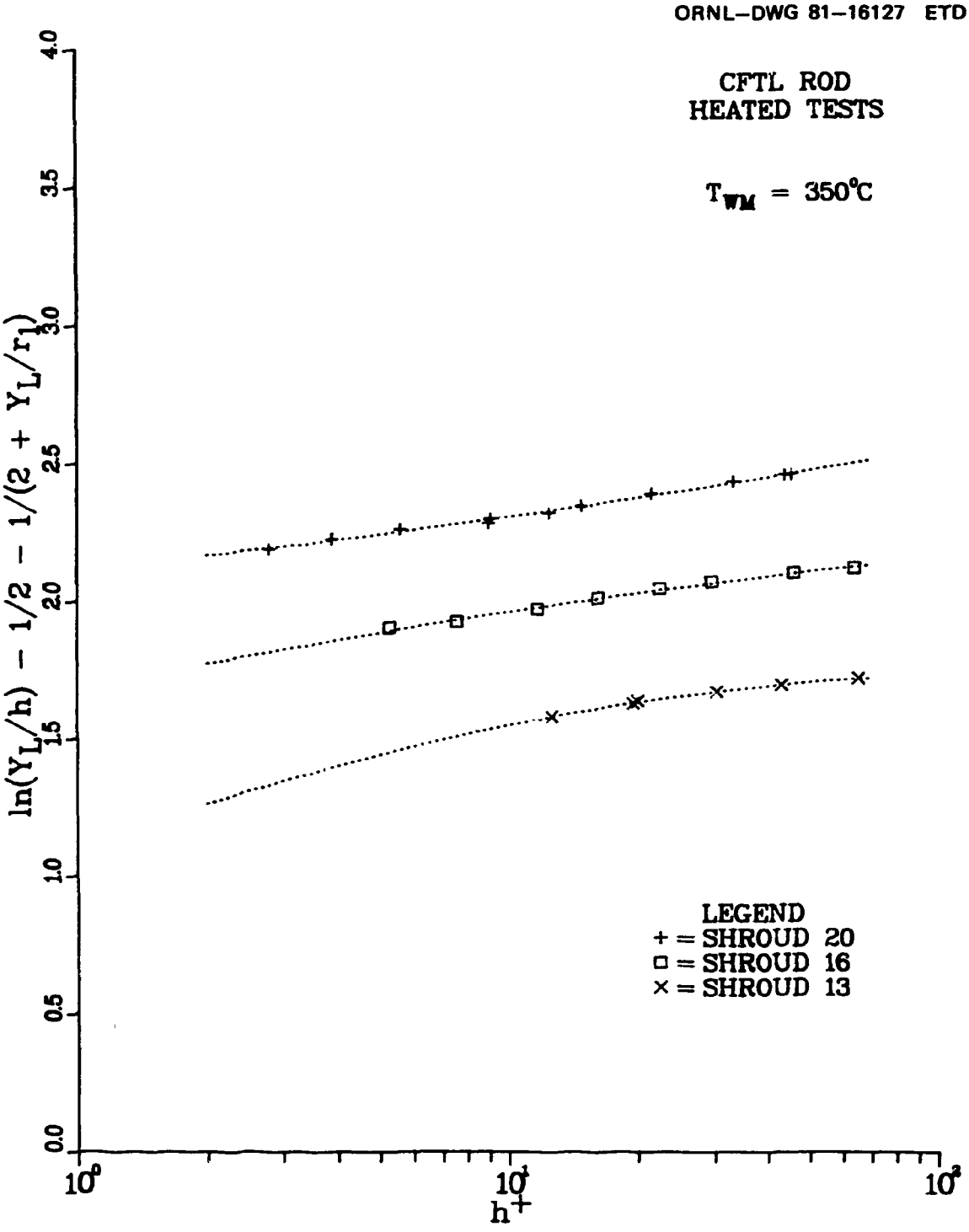

Fig. 12. Variation of abscissa values with roughness Reynolds number in the transition zone.

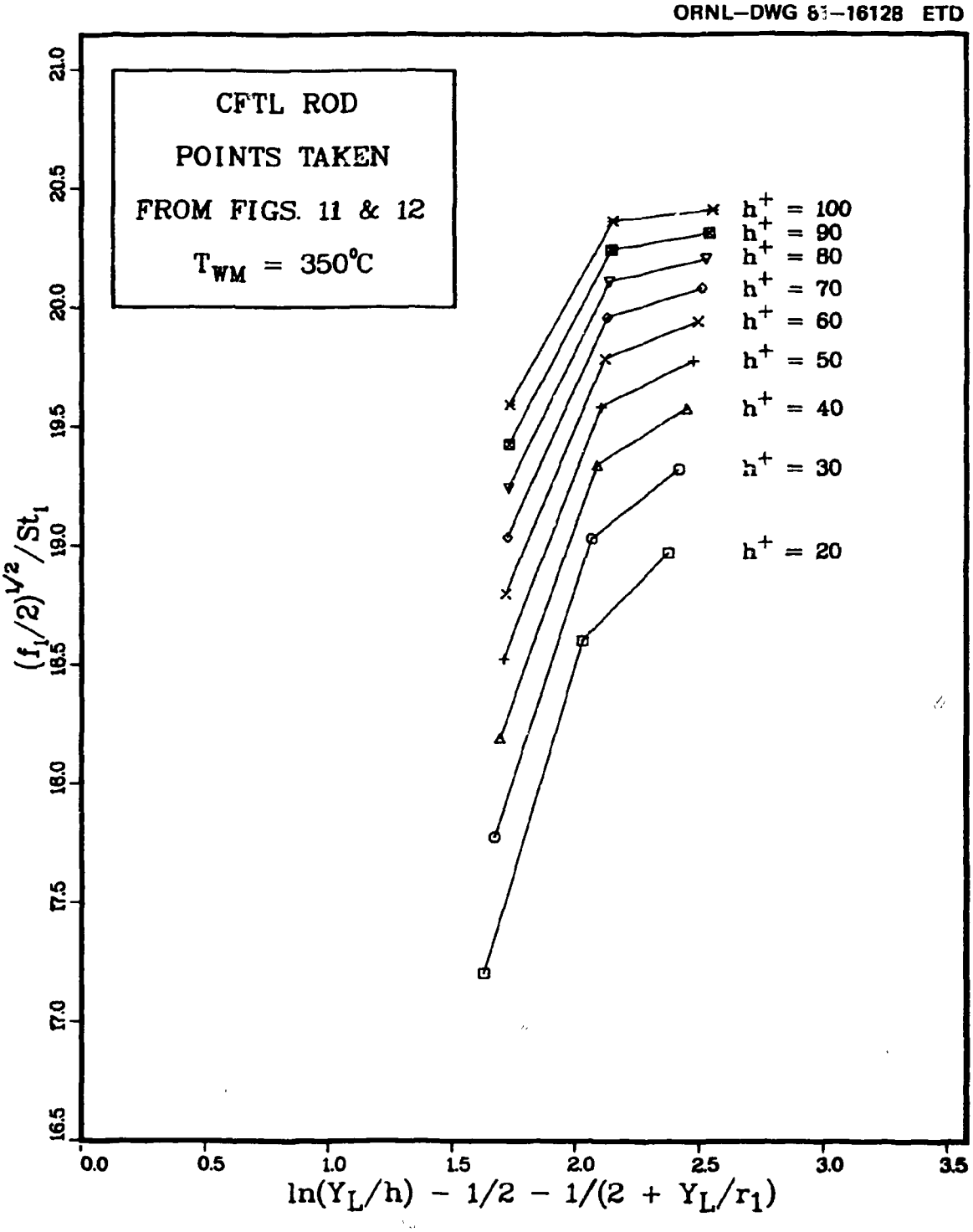

Fig. 13. Universal law of heat transfer for CFTL rod.

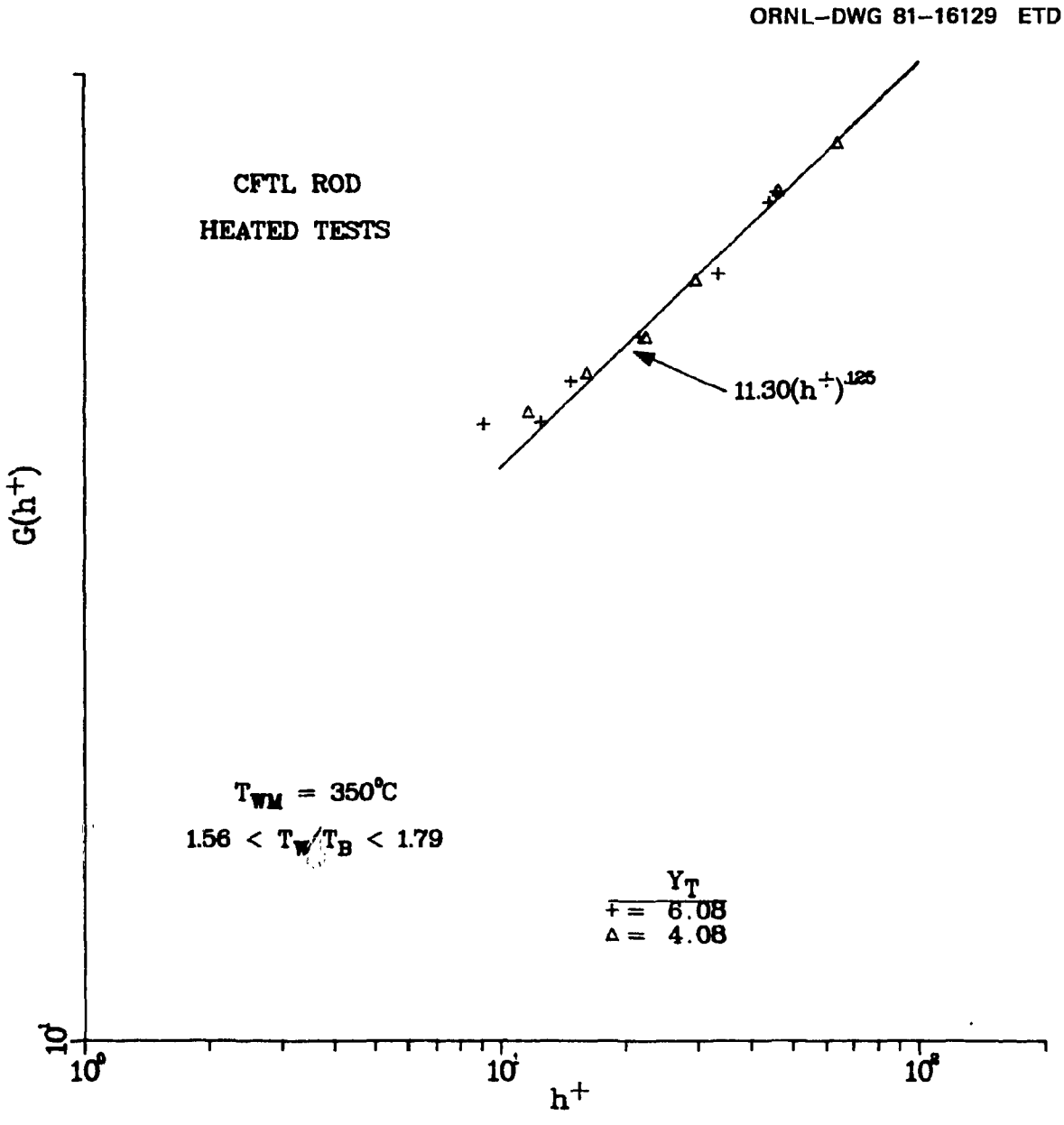

Fig. 14. Correlation for G(h$^+$) using slopes determined graphically for the CFTL rod.

Table 5. Slopes A_H and intercepts for the straight lines connecting points representing the 16-mm and 20-mm annular geometries of Fig. 13

h^+	A_H	$G(h^+)$
20	1.067	16.438
30	0.833	17.312
40	0.660	17.962
50	0.524	18.482
60	0.417	18.903
70	0.325	19.266
80	0.245	19.585
90	0.178	19.861
100	0.118	20.110

those derived from the results of the heated tests for which the heat balance error was no more than five percent.

CONCLUSIONS

Correlations have been established for use in the calculation of both pressure drop and heat transfer for flow in the various channels of the proposed CFTL bundle. The nature and use of these correlations will be summarized in this section.

For fully rough flow, the friction factor under both heated and isothermal conditions can be calculated by use of Eq. (2) with the constant values

$$A = 2.96 , \tag{20}$$

and

$$R(h^+) = 4.45 . \tag{21}$$

The development of these values from the experimental results is shown in Fig. 1.

With the friction factor known, the Stanton number in fully rough flow can be determined by use of Eq. (12). The values of A_H and $G(h^+)$ for use in this equation depend upon the temperatures and temperature differences associated with the flow, which can be characterized by the maximum rod wall temperature T_{WM}. For a T_{WM} of 150° C, A_H is given by Eq. (17) while $G(h^+)$ can be read from Fig. 10 or calculated from the relation

$$G(h^+) = 11.61(h^+)^{0.078} . \tag{22}$$

For a T_{WM} of 350° C, A_H is given by Eq. (19) and $G(h^+)$ can be taken from Fig. 14 or calculated using the relation

$$G(h^+) = 11.30(h^+)^{0.0125} . \tag{23}$$

For conditions characterized by maximum rod wall temperatures other than the 150 and 350° C employed in this experiment, it is recommended that the results of these correlations be used in the process of linear interpolation or extrapolation as necessary to calculate values appropriate to the desired temperatures.

In this work, the limits of the transition from hydraulically smooth to fully rough turbulent flow have been well established for the CFTL roughness in terms of the roughness Reynolds number (h^+). For flow channels with physical dimensions near those of the proposed CFTL bundle, the transition zone begins at an h^+ value at about 4.0 and continues to an h^+ value of about 20.0 as shown on Fig. 2.

For flow in the transition zone, the friction factor can again be calculated through use of Eq. (2). In this flow regime, the parameter A was found to remain constant at the same value as for fully rough flow (Eq. 20). However, the parameter $R(h^+)$ was found to be a function of the roughness Reynolds number and can be calculated using Eq. (9).

With the friction factor known, the Stanton number in the transition zone can be easily determined through use of simple expressions for the term

$$\sqrt{f_t/2}/St_t\,, \tag{24}$$

which is independent of velocity profile width in this flow regime. As shown in Fig. (7), a value of 16.58 is appropriate for transitional zone flow at a T_{WM} of 150° C. For flow at a T_{WM} of 350° C, this term is well represented by the relation

$$\sqrt{f_t/2}/St_t = 21.10\,(h^+)^{-0.067} \tag{25}$$

as shown in Fig. 11.

SUMMARY

Several different universal velocity profile widths would exist simultaneously in the different channels within the roughened portion of the CFTL bundle design. A successful analysis of the distribution of these channel flows depends upon prior determination of the behavior of the friction factor and Stanton number as functions of the velocity profile width for the particular CFTL roughness.

In this report, the results of an experiment performed at Kernforschungszentrum Karlsruhe to determine the friction factor and Stanton number behavior characteristics of a prototype CFTL roughened rod are presented. The methods described in an earlier work[1] are implemented to convert the experimental results into correlations for the roughness friction factor parameters A and $R(h^+)$ and the roughness heat transfer parameters A_H and $G(h^+)$.

The dependence of these four roughness parameters upon the roughness Reynolds number h^+ was experimentally determined by testing a single prototypic CFTL roughened rod in a series of three annular geometries. The three test annular geometries were formed by placing the roughened CFTL rod successively at the center of each of three smooth outer shroud tubes of different diameter. The Dalle Donne-Meyer transformation[6] was used for calculation of both the location of the surface of zero shear in the flow and the friction factor associated with the rough surface.

The results of this experimental and analytical effort are conclusive in establishing the roughness parameters for determination of the friction factors in the various channels of the CFTL bundle design, both for fully rough and transitional zone flow. The test results indicate that the isothermal friction factor correlations are valid for heated flow as well as for isothermal flow, for flows in small annular geometries such as that associated with the bundle dimensions of the CFTL.

The experimental results for the determination of the heat transfer parameters are less conclusive. Heat transfer correlations for the determination of Stanton number are recommended for flows past

rods of the CFTL design with maximum rod wall temperatures of 150° C and 350° C. These correlations can be used for interpolation or extrapolation as necessary to determine the Stanton number for flows within the CFTL bundle at different maximum rod wall temperatures.

NOMENCLATURE

A	Slope of Eq. (2); mathematically equivalent to slope of dimensionless velocity profile
A_{II}	Slope of Eq. (12); mathematically equivalent to slope of dimensionless temperature profile
C_1, C_2, C_3	Constants in Eq. (6)
C_4, C_5, C_6	Constants in Eq. (7)
C_p	Specific heat at constant pressure
D	Equivalent diameter
f	Fanning friction factor
$G(h^+)$	Heat transfer roughness parameter for a particular fluid
h	Height of roughness element
h^+	Roughness Reynolds number ($=\frac{hu^*}{\nu}$) based on the viscosity at the temperature at the wall
q_w	Heat flux at the wall
r	Radius
Re	Reynolds number
$R(h^+)$	Roughness parameter for frictional pressure loss
St	Stanton number
T_B	Bulk coolant temperature
T_w	Temperature at the wall
T_{mm}	Maximum measured temperature along the rough wall
$\bar{u}$	Spacially averaged axial velocity
u^*	Friction velocity ($=\sqrt{\tau_w/\rho}$)
$\bar{u}^+$	Average value of dimensionless velocity ($=\bar{u}/u^*$)
Y_L	Velocity profile width, from volumetric surface of rough wall to surface of zero shear
Y_T	Annular gap, distance in annular test geometry from volumetric surface of rough wall to smooth surface

Greek Symbols

α	Radius ratio of annulus ($= r_1/r_2$)
β	Ratio of radius of surface of zero shear in annular test geometry to radius of smooth tube wall ($= r_0/r_2$)
ρ	Density
τ	Shear stress at the wall
ν	Kinematic viscosity

Subscripts

0	Pertaining to the surface of zero shear
1	Pertaining to the rough surface, or to the zone of flow in annular geometry between the rough surface and the surface of zero shear
2	Pertaining to the smooth tube wall in annular test geometry

REFERENCES

1. S. A. Hodge, "Determination of Coefficients for the Universal Laws of Friction and Heat Transfer for CFTL Calculations," ORNL/TM-7418 (1980).

2. S. A. Hodge, J. P. Sanders, and D. E. Klein, "Determination of Friction Factors and Heat Transfer Coefficients for Flow Past Articifically Roughened Surfaces," ORNL-5599 (1979).

3. J. Nikuradse, "Laws of Flow in Rough Pipes," NACA TM 1292 (1950).

4. S. A. Hodge, J. P. Sanders, and D. E. Klein, "Slope and Intercept of the Dimensionless Velocity Profile for Articifically Roughened Surfaces," Int. J. Heat Mass Transfer, 23, 135–140 (1980).

5. L. Meyer and L. Vogel, "The Velocity Distribution and Pressure Loss of Artificial Roughnesses with Sharp and Rounded Edges," KfK 2885 (1979).

6. M. Dalle Donne and L. Meyer, "Turbulent Convective Heat Transfer from Rough Surfaces with Two-Dimensional Rectangular Ribs," Int. J. Heat Mass Transfer, 20, 583–620 (1977).

7. M. Dalle Donne, "Heat Transfer from Rough Surfaces," Report KfK 2397, EUR 5506d (1977) (in German).

8. L. Meyer, "Heat Transfer and Pressure Drop at Single Rods with Three-Dimensional Roughnesses: Large Scale Tests," Report KfK 3164 (1981).

9. M. Dalle Donne and L. Meyer, "Heat Transfer and Pressure Drop at Single Rods Roughened with Three-Dimensional Ribs," OCED-NEA 6th GCFR Heat Transfer Specialists Meeting, Berkeley, England (1980).

10. L. Meyer, "Friction and Heat Transfer Correlations for the Roughness of the BR2 Calibration Element," Report KfK 2986 (1980).

11. L. Meyer and K. Rehme, "Heat Transfer and Pressure Drop Measurements with Roughened Single Pins Cooled by Various Gases, Report KfK 2980 (1980).

Appendix A

PHOTOMICROGRAPH OF CFTL CLADDING SURFACE

MC-IC-0

INTRA-LABORATORY CORRESPONDENCE

OAK RIDGE NATIONAL LABORATORY

March 4, 1981

To: John P. Sanders
Building 9108, Mail Stop 2, Room 203, Y-12

From: R. J. Gray

Subject: Photomicrograph 75x, Longitudinal Profile of Centerless Ground, Type 316 SS Tubing.

Enclosed are 6 prints of the subject examination. You expressed a primary interest in the profile of the grinding operation. The microstructure shows some mechanical twinning across the entire tube wall. This twinning undoubtedly was produced in a cold working step--probably during a drawing or straightening operation. The grinding operation did not produce localized cold working at the surface. The absence of cold working indicates a careful grinding procedure.

RJG/blh

Enclosure

Etchant: Electrolyte 40% HNO_3 in water, 0.01 amps/CM^2

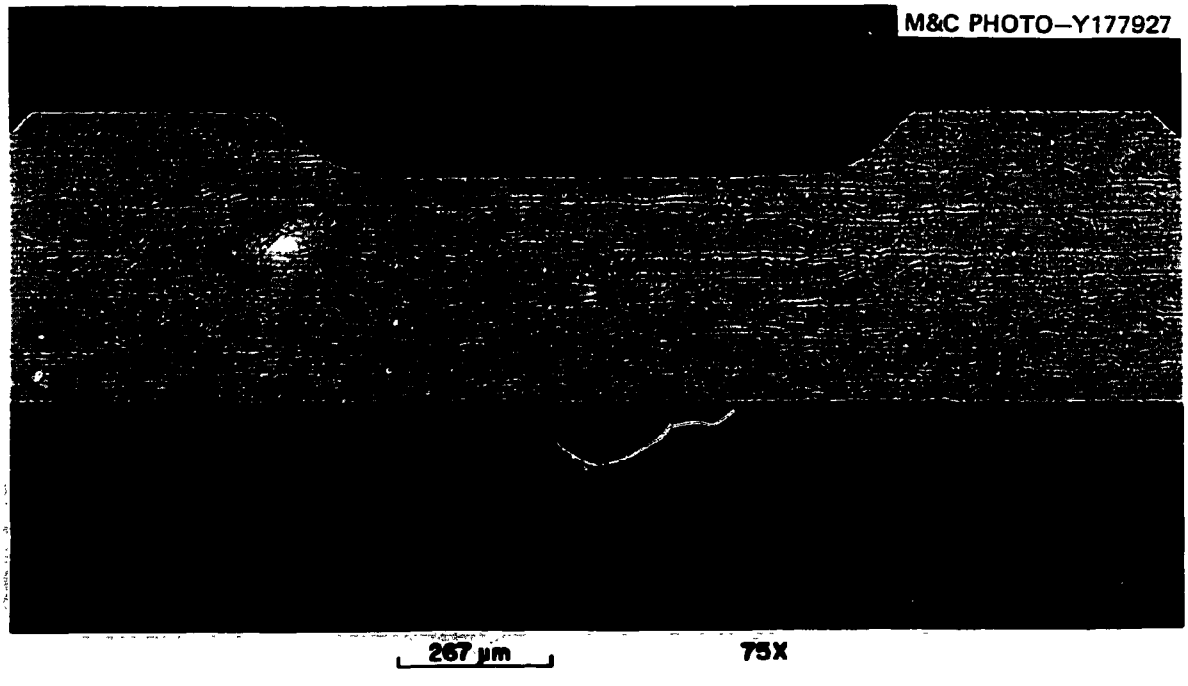

Appendix B

EXPERIMENTAL APPARATUS AND PROCEDURE

The experiment was performed in an air test rig at Kernforschungszentrum Karlsruhe (KfK). The apparatus and the experimental techniques were similar to those previously used in both large scale and small scale tests.[7-11]

A schematic diagram of the experimental apparatus used for the CFTL rod experiment is shown in Fig. B-1. Air is circulated through this open loop by a compressor; the pressure pulsations are damped in a large holdup tank. An air drier reduces the humidity of the air. Air flow is measured by one of four available orifice flowmeters placed in parallel and calibrated over various ranges of mass flow. After passing through the annular test section, the air is released through a silencer to the atmosphere. The apparatus is capable of a maximum mass flow of 90 grams/s, at a maximum pressure of five atmospheres.

The test series involved both the isothermal and heated axial flow of air past the roughened CFTL rod surface successively placed in three different annular geometries. The annular flow channels were each formed by placing the rough rod at the center of one of three smooth tubes of varying diameter. One smooth tube of 20-mm I.D. and another of 16-mm I.D. were supplied for these tests by KfK; the third smooth tube of 13.08-mm I.D. was supplied by ORNL and subsequently straightened and honed at KfK before use.

The pressure gradient along the test section was measured at eight static pressure taps spaced at 80 mm intervals along the surface of the smooth tube. The location of the static pressure taps and the placement of the 7.82-mm diameter CFTL rod within the smooth outer tube of 16-mm diameter are shown in Fig. B-2. The absolute and differential pressures were measured by five capacitance-type pressure transducers (MKS-Baratron) with an accuracy of better than 1% over the range from 1 to 10^6 Pa.

For the heated tests, temperatures were measured by sheathed Nickel-Chromium/Nickel-Alumel thermocouples. The CFTL rod wall temperature profile was measured by 14 thermocouples placed at 10 different axial locations along the rod; two thermocouples were placed on opposite sides of the rod at four locations so that any rod bowing would be indicated by a significant temperature difference. The outer surface of each smooth tube was insulated by a thick layer of Kerlane tape and the tube wall temperature was measured by 16 thermocouples placed at 8 axial locations. Three additional thermocouples were placed to measure the air bulk temperature in a mixing chamber at the test section outlet. The rod power, which can be varied from 0 to 13 kW, was adjusted as necessary to keep the maximum rod wall temperature constant during each series of test runs at different mass flows.

The spacers located between the first and second and between the seventh and eighth pressure taps as shown on Fig. B-2 were used only for the tests in the 13-mm and the 16-mm smooth outer tubes. The purpose of these spacers was to avoid test inaccuracies introduced by rod bowing when there is a small clearance between the rod wall and the inner tube wall. The spacers consisted of three thin pieces of metal which were laser-beam welded directly to the rod surface. The spacer tips were insulated from the inner tube wall by a ceramic layer.

A heat balance was performed for all non-isothermal runs to compare the measured electrical input power to the rod with the thermal power calculated from the measured mass flow and air temperature increase. Only data for the runs in which the difference in the electrical and thermal powers was less than 6% were retained for further analyses.

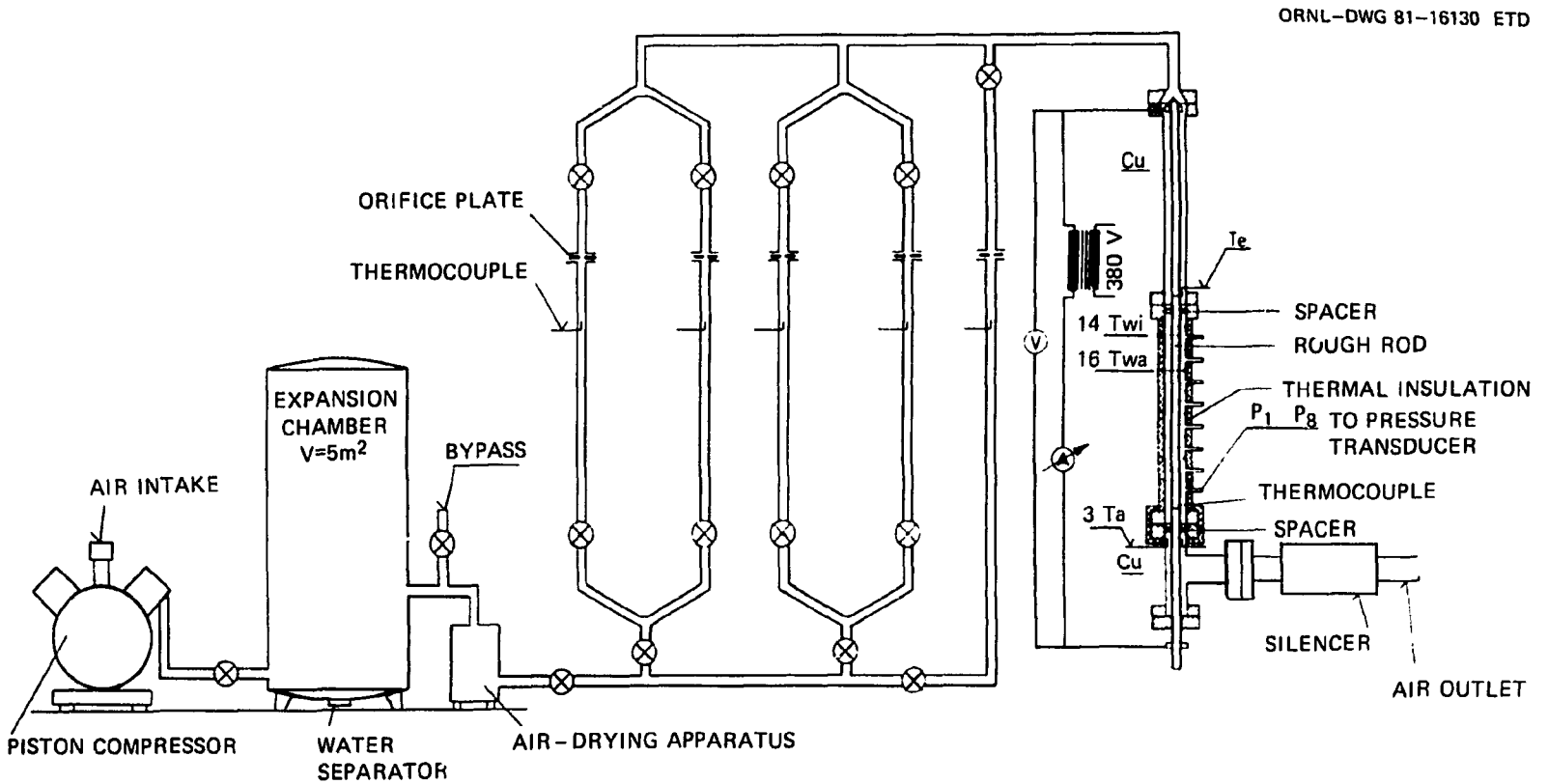

Fig. B-1. Apparatus used for the KfK air tests of the CFTL rod.

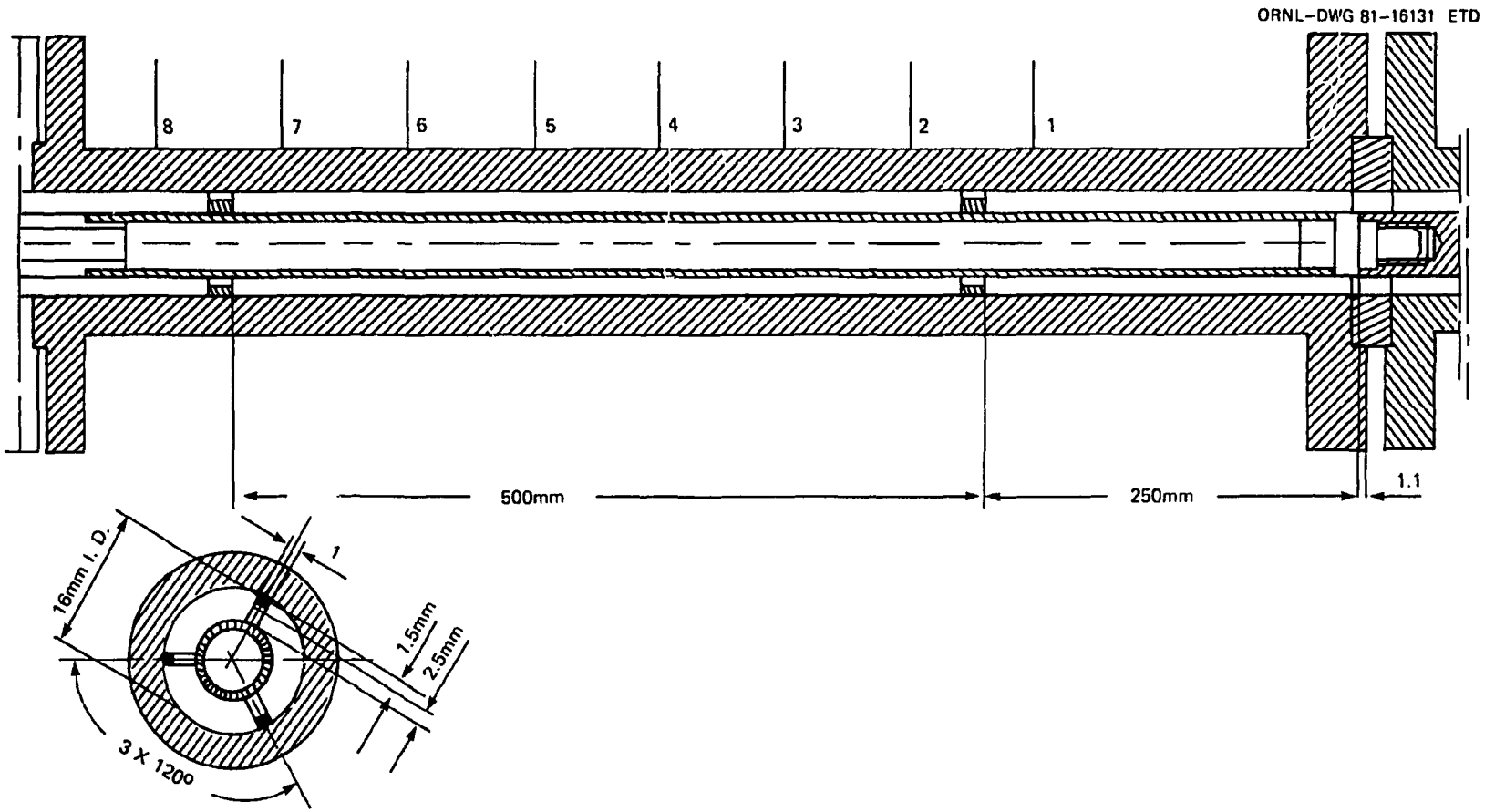

Fig. B-2. Placement of the CFTL rod within the smooth tube.

The test data were processed at ORNL using the KfK code AURIS, which converts the experimentally measured values of pressure and temperature at several axial locations along the test section into an overall friction factor and Stanton number for the rough rod-smooth tube combination. The subsequent transformation of these values into the friction factor and Stanton number applicable to the region between the rough surface and the surface of zero shear in the adjacent flow is also performed by AURIS.

Appendix C

EXPERIMENTAL RESULTS

EXPERIMENTAL RESULTS—ISOTHERMAL TESTS

Shroud	Test No.	$Re \times 10^{-4}$	f	Y_1 h	h'	f_1	Eq. (4)	$\sqrt{2/f_1}$
20	1	24.46	0.00697	29.48	211.5	0.01368	2.548	12.090
	2	19.91	0.00723	29.39	174.9	0.01413	2.545	11.898
	3	17.04	0.00738	29.23	150.7	0.01432	2.539	11.818
	4	14.64	0.00753	29.06	130.2	0.01448	2.532	11.751
	5	11.81	0.00766	28.65	105.0	0.01444	2.516	11.768
	6	11.10	0.00765	28.43	98.1	0.01427	2.508	11.840
	7	10.16	0.00778	28.40	90.5	0.01450	2.507	11.745
	8	7.38	0.00802	27.79	65.8	0.01448	2.482	11.754
	9	6.43	0.00811	27.47	57.2	0.01439	2.470	11.791
	10	5.91	0.00821	27.37	52.8	0.01450	2.466	11.744
	11	4.74	0.00849	27.09	42.7	0.01477	2.454	11.636
	12	3.84	0.00859	26.48	34.4	0.01445	2.429	11.764
	13	3.12	0.00891	26.24	28.2	0.01479	2.419	11.631
	14	2.71	0.00890	25.64	24.1	0.01427	2.393	11.837
	15	2.30	0.00931	25.72	21.0	0.01502	2.397	11.540
	16	1.99	0.00938	25.23	18.1	0.01470	2.375	11.665
	17	1.67	0.00950	24.64	15.0	0.01438	2.350	11.795
	18	1.21	0.00985	23.73	10.8	0.01409	2.308	11.916
	19	1.20	0.00976	23.52	10.6	0.01377	2.298	12.052
	20	0.88	0.01022	22.73	7.7	0.01370	2.261	12.084
	21	0.63	0.01061	21.61	5.5	0.01319	2.205	12.314
	22	0.47	0.01057	19.61	3.9	0.01137	2.099	13.264
	23	0.34	0.01000	15.58	2.4	0.00774	1.847	16.073
	24	0.26	0.00976	11.82	1.5	0.00520	1.545	19.610
	25	0.19	0.01246	16.75	1.5	0.01058	1.927	13.748
16	1	13.38	0.00877	20.89	188.9	0.01655	2.168	10.992
	2	7.42	0.00931	20.30	106.0	0.01691	2.136	10.876
	3	4.60	0.00980	19.78	66.3	0.01720	2.108	10.783
	4	3.25	0.01014	19.33	47.0	0.01725	2.083	10.767
	5	2.20	0.01063	18.86	32.0	0.01748	2.056	10.696
	6	1.68	0.01080	18.34	24.3	0.01708	2.026	10.821
	7	1.22	0.01107	17.71	17.4	0.01666	1.988	10.957
	8	1.21	0.01107	17.70	17.3	0.01665	1.987	10.960
	9	0.91	0.01152	17.28	13.0	0.01675	1.961	10.928
	10	0.66	0.01178	16.51	9.3	0.01605	1.912	11.164
	11	0.50	0.01166	15.42	6.7	0.01440	1.838	11.786
	12	0.33	0.01189	13.99	4.2	0.01281	1.732	12.496
	13	0.33	0.01157	13.63	4.1	0.01202	1.703	12.902
	14	0.24	0.01184	12.54	2.9	0.01097	1.612	13.499
	15	0.19	0.01341	13.18	2.5	0.01319	1.668	12.312
	16	0.14	0.01790	15.60	2.3	0.02242	1.850	9.444
	17	0.09	0.02758	18.50	2.1	0.04485	2.035	6.678
13	1	8.75	0.01166	14.38	220.1	0.02192	1.762	9.553
	2	5.21	0.01215	14.04	131.9	0.02215	1.736	9.502
	3	5.00	0.01226	14.04	127.2	0.02237	1.736	9.455
	4	3.12	0.01276	13.69	79.6	0.02255	1.709	9.417
	5	2.16	0.01324	13.42	55.5	0.02284	1.688	9.357
	6	1.48	0.01381	13.13	38.3	0.02317	1.664	9.291
	7	1.48	0.01371	13.10	38.2	0.02292	1.662	9.341
	8	1.07	0.01411	12.79	27.6	0.02288	1.636	9.350
	9	0.76	0.01432	12.36	19.4	0.02217	1.599	9.497
	10	0.51	0.01435	11.68	12.6	0.02058	1.539	9.858
	11	0.37	0.01485	11.29	9.1	0.02031	1.502	9.923
	12	0.37	0.01428	11.06	8.9	0.01899	1.481	10.261
	13	0.28	0.01434	10.44	6.4	0.01762	1.420	10.653
	14	0.20	0.01352	9.13	4.1	0.01382	1.276	12.031
	15	0.14	0.01813	10.54	3.7	0.02259	1.429	9.410
	16	0.10	0.02602	11.91	3.3	0.03872	1.560	7.187

EXPERIMENTAL RESULTS—HEATED TESTS—T_{WM} = 150°C

Shroud	Test No.	Re × 10^{-4}	f	Y_1/h	h^*	f_1	Eq. (4)	$\sqrt{2/f_1}$
20	1	15.80	0.00716	28.30	81.8	0.01366	2.502	12.099
	2	10.06	0.00752	27.56	52.6	0.01384	2.473	12.021
	3	6.87	0.00778	26.75	36.0	0.01373	2.440	12.068
	4	5.21	0.00797	26.13	27.3	0.01366	2.414	12.101
	5	3.47	0.00826	25.07	18.1	0.01330	2.368	12.264
	6	2.38	0.00875	24.45	12.7	0.01360	2.341	12.126
	7	1.27	0.00947	22.87	6.8	0.01335	2.267	12.238
	8	1.13	0.00979	22.89	6.1	0.01380	2.268	12.039
	9	0.94	0.00996	22.24	5.0	0.01348	2.236	12.179
	10	0.75	0.01030	21.69	4.1	0.01342	2.209	12.208
	11	0.60	0.01062	20.99	3.2	0.01322	2.173	12.300
	12	0.46	0.01074	19.55	2.4	0.01210	2.095	12.854
	13	0.36	0.01023	16.53	1.6	0.00916	1.912	14.774
	14	0.26	0.01218	18.03	1.4	0.01331	1.977	12.258
	15	0.30	0.01076	13.73	1.3	0.00955	1.514	14.472

Shroud	Test No.	S_t	T_W/T_B	$\frac{T_W-T_{BI}}{TW-TB}$	β	S_{t_1}	$\sqrt{2/f_1}S_{t_1}$	Heat balance error(÷)
20	1	0.00400	1.342	0.933	0.760	0.00438	18.849	1.7
	2	0.00417	1.341	0.926	0.751	0.00460	18.075	0.5
	3	0.00426	1.338	0.919	0.740	0.00472	17.531	1.0
	4	0.00439	1.337	0.916	0.732	0.00488	16.929	0.5
	5	0.00430	1.335	0.906	0.718	0.00481	16.951	1.4
	6	0.00438	1.328	0.901	0.710	0.00492	16.761	0.6
	7	0.00442	1.326	0.885	0.690	0.00502	16.293	3.0
	8	0.00437	1.324	0.886	0.690	0.00494	16.820	2.1
	9	0.00441	1.331	0.880	0.682	0.00501	16.379	4.6
	10	0.00435	1.319	0.879	0.674	0.00494	16.596	5.2
	11	0.00423	1.327	0.881	0.665	0.00477	17.044	7.0
	12	0.00410	1.328	0.875	0.647	0.00463	16.816	9.8
	13	0.00377	1.333	0.854	0.607	0.00429	15.777	12.3
	14	0.00384	1.315	0.888	0.627	0.00434	18.794	17.6
	15	0.00374	1.309	0.638	0.571	0.00608	11.363	15.9

Shroud	Test No.	Re × 10^{-4}	f	Y_L/h	h^*	f_1	Eq. (4)	$\sqrt{2/f_1}$
16	1	11.88	0.00882	20.59	108.5	0.01673	2.152	10.933
	2	7.42	0.00905	19.92	68.3	0.01645	2.116	11.027
	3	5.32	0.00934	19.53	49.5	0.01655	2.094	10.993
	4	3.33	0.00981	18.96	31.5	0.01671	2.062	10.941
	5	2.13	0.01000	18.03	19.8	0.01590	2.007	11.217
	6	1.59	0.01048	17.77	15.1	0.01638	1.991	11.051
	7	1.16	0.01074	17.12	10.8	0.01596	1.951	11.195
	8	1.14	0.01073	17.07	10.7	0.01588	1.948	11.222
	9	0.82	0.01135	16.72	7.8	0.01633	1.925	11.066
	10	0.59	0.01164	15.93	5.6	0.01567	1.873	11.298
	11	0.47	0.01138	14.81	4.2	0.01385	1.793	12.018
	12	0.35	0.01144	13.78	3.0	0.01270	1.714	12.550
	13	0.31	0.01182	13.64	2.7	0.01293	1.703	12.435

HEATED TESTS—T_{wall} = 150°C (cont'd)

Shroud	Test No.	S_t	$T_w - T_B$	$\frac{T_w - T_{Bi}}{TW - TB}$	β	S_{t_1}	$\sqrt{2 f_i} S_{t_1}$	Heat balance error(%)
16	1	0.00435	1.288	0.951	0.825	0.00471	19.432	0.2
	2	0.00463	1.276	0.943	0.814	0.00505	17.974	0.9
	3	0.00476	1.271	0.941	0.808	0.00520	17.497	1.1
	4	0.00480	1.263	0.936	0.798	0.00526	17.363	2.8
	5	0.00482	1.262	0.924	0.783	0.00533	16.718	2.5
	6	0.00493	1.258	0.928	0.779	0.00543	16.663	0.3
	7	0.00494	1.263	0.921	0.769	0.00546	16.346	1.3
	8	0.00496	1.256	0.921	0.768	0.00549	16.245	2.0
	9	0.00494	1.258	0.923	0.762	0.00545	16.594	4.8
	10	0.00486	1.252	0.918	0.749	0.00536	16.513	7.6
	11	0.00462	1.256	0.909	0.731	0.00509	16.332	9.7
	12	0.00418	1.255	0.927	0.714	0.00452	17.636	12.0
	13	0.00402	1.245	0.938	0.712	0.00429	18.753	11.2

Shroud	Test No.	$Re \times 10^{-4}$	f	Y_i h	h'	f_i	Eq (4)	$\sqrt{2 f_i}$
13	1	8.06	0.01153	14.22	145.7	0.02177	1.750	9.584
	2	5.35	0.01206	14.00	101.6	0.02236	1.733	9.457
	3	3.44	0.01249	13.67	65.6	0.02253	1.708	9.421
	4	2.16	0.01310	13.34	41.9	0.02294	1.681	9.338
	5	1.90	0.01307	13.16	36.7	0.02248	1.667	9.432
	6	1.88	0.01310	13.14	36.0	0.02243	1.665	9.441
	7	1.30	0.01343	12.79	25.2	0.02228	1.636	9.475
	8	0.82	0.01353	12.14	15.4	0.02104	1.580	9.749
	9	0.54	0.01342	11.37	9.7	0.01918	1.510	10.212
	10	0.36	0.01344	10.64	6.2	0.01766	1.440	10.641
	11	0.35	0.01354	10.59	6.0	0.01766	1.435	10.641
	12	0.26	0.01293	9.67	4.0	0.01515	1.337	11.492

Shroud	Test No.	S_t	$T_w - T_B$	$\frac{T_w - T_{Bi}}{TW - TB}$	β	S_{t_1}	$\sqrt{2 f_i} S_{t_1}$	Heat balance error(%)
13	1	0.00495	1.205	0.984	0.882	0.00523	19.953	0.3
	2	0.00541	1.179	0.984	0.878	0.00572	18.499	0.5
	3	0.00572	1.179	0.980	0.871	0.00607	17.490	0.6
	4	0.00589	1.174	0.977	0.865	0.00626	17.109	1.0
	5	0.00598	1.172	0.970	0.861	0.00640	16.577	1.3
	6	0.00581	1.176	0.959	0.861	0.00627	16.902	0.3
	7	0.00611	1.167	0.968	0.854	0.00654	16.148	2.4
	8	0.00620	1.167	0.971	0.841	0.00659	15.559	5.3
	9	0.00609	1.169	0.971	0.826	0.00645	15.176	9.6
	10	0.00536	1.184	0.986	0.811	0.00557	16.864	15.2
	11	0.00537	1.173	0.991	0.810	0.00555	16.939	12.9
	12	0.00432	1.195	1.041	0.792	0.00425	20.480	24.3

EXPERIMENTAL RESULTS—HEATED TESTS—T_{wall} 350 C

Shroud	Test No	Re × 10^{-4}	f	Y_1 h	h'	f_1	Eq (4)	$\sqrt{2 f_1}$
20	1	25 72	0 00604	26.89	74 2	0 01122	2.445	13.351
	2	14 54	0 00693	27 25	45 6	0 01310	2 460	12 355
	3	14.11	0.00693	27 16	44 0	0 01306	2 457	12 375
	4	10 62	0.00712	26 62	33 4	0 01308	2.434	12 366
	5	6.88	0.00737	25 58	21 6	0 01282	2 390	12.492
	6	4.70	0.00760	24.62	14 8	0 01256	2 348	12 619
	7	3 99	0.00768	24.04	12.5	0 01226	2.322	12.775
	8	2.80	0.00817	23.60	9 1	0 01267	2 301	12 562
	9	2.81	0 00802	23 24	9.0	0.01217	2.284	12.821
	10	1.69	0 00869	22.78	5.6	0.01305	2.262	12.379
	11	1.15	0.00950	22.07	3.9	0.01329	2.227	12 267
	12	0.82	0.01005	21.34	2.8	0.01333	2.191	12.248
	13	0.61	0 01065	20.91	2 1	0 01374	2.168	12.063
	14	0 47	0.01154	20.99	1.7	0.01520	2.169	11.469
	15	0.34	0.01081	17.70	1 1	0 01125	1.986	13.336

Shroud	Test No.	S_1	T_w T_B	$\frac{T_w - T_{BI}}{T_W - T_B}$	β	S_{12}	$\sqrt{2 f_1} S_{12}$	Heat balance error(%)
20	1	0.00346	1.795	0.933	0.743	0.00381	19 636	13.1
	2	0 00370	1.789	0.935	0.748	0.00408	19.832	1.1
	3	0.00371	1 792	0.934	0.747	0.00409	19.755	0.9
	4	0.00380	1.785	0.930	0.740	0.00416	19.250	0.5
	5	0.00380	1.781	0.924	0.726	0.00418	18.973	0.5
	6	0 00380	1 769	0.919	0.714	0.00418	18.742	0.0
	7	0.00381	1.769	0.911	0.706	0.00433	18.368	0 5
	8	0.00385	1.754	0.908	0.700	0.00422	18 493	1.6
	9	0.00385	1.745	0.902	0.696	0.00447	18.068	1.2
	10	0.00384	1.745	0.900	0.690	0.00434	18.797	1.3
	11	0.00382	1.744	0.895	0.680	0.00428	19.074	3.5
	12	0.00371	1.735	0.893	0.671	0.00420	19.737	4.9
	13	0.00357	1.742	0.901	0.665	0.00395	20.979	8.1
	14	0.00358	1.723	0.911	0.666	0.00396	22.000	10.7
	15	0.00329	1.710	0.903	0.624	0.00362	20.738	15.0

Shroud	Test No	Re × 10^{-4}	f	Y_1 h	h'	f_1	Eq. (4)	$\sqrt{2 f_1}$
16	1	10.63	0.00851	19.99	64.0	0.01614	2.119	11.131
	2	7.48	0.00886	19.66	46.2	0.01644	2.101	11.028
	3	4.78	0.00920	19.11	29.7	0.01658	2.070	10.983
	4	3.57	0.00941	18.66	22.5	0.01643	2.044	11.033
	5	2.55	0.00967	18.12	16.2	0.01623	2.012	11.100
	6	1.87	0.00983	17.46	11.7	0.01572	1.972	11.280
	7	1.22	0.01031	16.73	7.6	0.01549	1.925	11.364
	8	1.21	0.01033	16.73	7.6	0.01551	1.925	11.357
	9	0.83	0.01113	16.42	5.3	0.01628	1.905	11.084
	10	0.61	0.01147	15.83	4.0	0.01597	1.866	11.189
	11	0 43	0.01154	14.76	2.6	0.01472	1.789	11.657
	12	0.31	0.01230	14.59	2.0	0.01560	1.777	11.322
	13	0.27	0.01217	14.08	1.6	0.01491	1.739	11.582

HEATED TESTS—$T_{w,i}$ = 350°C (cont'd)

Shroud	Test No.	S	$T_w - T_B$	$\frac{T_w - T_{B_2}}{T_W - T_B}$	β	S_t	$\sqrt{2 f_i} S_t$	Heat balance error(%)
16	1	0.00417	1.630	0.960	0.816	0.00454	19.805	0.9
	2	0.00425	1.613	0.958	0.811	0.00462	19.622	1.2
	3	0.00439	1.609	0.959	0.802	0.00479	19.024	1.2
	4	0.00446	1.591	0.955	0.795	0.00486	18.587	0.8
	5	0.00447	1.584	0.949	0.786	0.00490	18.394	0.3
	6	0.00445	1.589	0.941	0.775	0.00490	18.097	1.0
	7	0.00431	1.593	0.930	0.763	0.00475	18.522	0.2
	8	0.00432	1.591	0.931	0.763	0.00477	18.449	0.2
	9	0.00431	1.581	0.933	0.758	0.00474	19.035	2.9
	10	0.00416	1.577	0.933	0.749	0.00455	19.635	4.6
	11	0.00378	1.589	0.945	0.731	0.00407	21.067	9.9
	12	0.00364	1.560	0.975	0.729	0.00386	22.868	10.7
	13	0.00338	1.583	0.997	0.720	0.00354	24.420	14.1

Shroud	Test No	$Re \times 10^{-4}$	f	Y_1 h	h'	t	Eq (4)	$\sqrt{2 f_i}$
13	1	4.59	0.01214	13.81	65.2	0.02272	1.718	9.383
	2	2.95	0.01259	13.51	43.2	0.02306	1.694	9.312
	3	2.04	0.01298	13.21	30.5	0.02318	1.670	9.289
	4	1.34	0.01349	12.81	20.1	0.02307	1.637	9.311
	5	1.30	0.01319	12.70	19.6	0.02248	1.628	9.433
	6	0.86	0.01333	12.14	12.7	0.02141	1.580	9.666
	7	0.61	0.01322	11.52	8.7	0.01992	1.524	10.021
	8	0.42	0.01237	10.36	5.3	0.01624	1.411	11.096
	9	0.30	0.01267	9.91	3.6	0.01593	1.364	11.204
	10	0.30	0.01258	9.91	3.6	0.01593	1.364	11.204
	11	0.23	0.01324	9.87	2.7	0.01697	1.359	10.857

Shroud	Test No.	S_t	$T_w - T_B$	$\frac{T_w - T_{B_2}}{T_W - T_B}$	β	S_t	$\sqrt{2 f_i} S_t$	Heat balance error(%)
13	1	0.00518	1.407	0.982	0.875	0.00554	19.247	0.4
	2	0.00557	1.382	0.991	0.869	0.00592	18.141	1.3
	3	0.00580	1.368	0.991	0.863	0.00618	17.428	1.9
	4	0.00561	1.364	0.975	0.855	0.00602	17.828	0.8
	5	0.00595	1.350	0.990	0.853	0.00633	16.744	4.3
	6	0.00579	1.351	0.980	0.842	0.00619	16.701	5.7
	7	0.00566	1.355	0.976	0.829	0.00606	16.470	8.6
	8	0.00484	1.377	0.968	0.807	0.00516	17.461	10.8
	9	0.00411	1.405	1.008	0.798	0.00423	21.076	14.2
	10	0.00421	1.399	1.021	0.798	0.00430	20.741	17.7
	11	0.00368	1.428	1.071	0.797	0.00368	25.019	22.7